Extensive Ca^{2+} leak through K4750Q cardiac ryanodine receptors caused by cytosolic and luminal Ca^{2+} hypersensitivity

Akira Uehara,[1]* Takashi Murayama,[4]* Midori Yasukochi,[2]* Michael Fill,[5] Minoru Horie,[6] Toru Okamoto,[7] Yoshiharu Matsuura,[7] Kiyoko Uehara,[3] Takahiro Fujimoto,[8] Takashi Sakurai,[4] and Nagomi Kurebayashi[4]*

[1]Department of Physiology, [2]Laboratory of Human Biology, and [3]Department of Cell Biology, Fukuoka University School of Medicine, Fukuoka 814-0180, Japan
[4]Department of Pharmacology, Juntendo University School of Medicine, Tokyo 113-8421, Japan
[5]Department of Molecular Biophysics and Physiology, Rush University Medical Center, Chicago, IL 60612
[6]Department of Cardiovascular and Respiratory Medicine, Shiga University of Medical Science, Shiga 520-2192, Japan
[7]Department of Molecular Virology, Research Institute for Microbial Diseases, Osaka University, Osaka 565-0871, Japan
[8]Department of Pathology and Applied Neurobiology, Graduate School of Medical Science, Kyoto Prefectural University of Medicine, Kyoto 602-8566, Japan

Various ryanodine receptor 2 (RyR2) point mutations cause catecholamine-induced polymorphic ventricular tachycardia (CPVT), a life-threatening arrhythmia evoked by diastolic intracellular Ca^{2+} release dysfunction. These mutations occur in essential regions of RyR2 that regulate Ca^{2+} release. The molecular dysfunction caused by CPVT-associated RyR2 mutations as well as the functional consequences remain unresolved. Here, we study the most severe CPVT-associated RyR2 mutation (K4750Q) known to date. We define the molecular and cellular dysfunction generated by this mutation and detail how it alters RyR2 function, using Ca^{2+} imaging, ryanodine binding, and single-channel recordings. HEK293 cells and cardiac HL-1 cells expressing RyR2-K4750Q show greatly enhanced spontaneous Ca^{2+} oscillations. An endoplasmic reticulum–targeted Ca^{2+} sensor, R-CEPIA1er, revealed that RyR2-K4750Q mediates excessive diastolic Ca^{2+} leak, which dramatically reduces luminal [Ca^{2+}]. We further show that the K4750Q mutation causes three RyR2 defects: hypersensitization to activation by cytosolic Ca^{2+}, loss of cytosolic Ca^{2+}/Mg^{2+}-mediated inactivation, and hypersensitization to luminal Ca^{2+} activation. These defects combine to kinetically stabilize RyR2-K4750Q openings, thus explaining the extensive diastolic Ca^{2+} leak from the sarcoplasmic reticulum, frequent Ca^{2+} waves, and severe CPVT phenotype. As the multiple concurrent defects are induced by a single point mutation, the K4750 residue likely resides at a critical structural point at which cytosolic and luminal RyR2 control input converge.

INTRODUCTION

In cardiac muscle, the Ca^{2+} influx through the surface membrane during the action potential activates ryanodine receptor 2 (RyR2) channels, a process called Ca^{2+}-induced Ca^{2+} release (CICR; Fabiato, 1983). During diastole, Ca^{2+} released by spontaneous single RyR2 openings may evoke localized inter-RyR2 CICR events (Stern, 1992), called Ca^{2+} sparks (Cheng et al., 1993). Sparks (and RyR2 openings that fail to evoke sparks) constitute the bulk of SR Ca^{2+} leak that normally limits diastolic SR Ca^{2+} overload. Diastolic RyR2 malfunction in catecholamine-induced polymorphic ventricular tachycardia (VT [CPVT]; Priori et al., 2001) is caused by single RyR2 point mutations. CPVT is an inherited disease in which frequent or large sparks can trigger propagating intracellular Ca^{2+} waves. These waves may drive sufficient diastolic Na^{+}-Ca^{2+} exchange to depolarize the surface membrane and evoke a delayed after-depolarization (DAD). DAD can lead to life-threatening VT. To date, all reported CPVT-linked RyR2 mutations are benign in resting individuals but elevate the risk of sudden cardiac death during exercise or emotional stress.

The fact that a point mutation in the RyR2, which has ~5,000 residues, may result in fatal cardiac arrhythmias implies that the mutated residue is essential for normal RyR2 operation. Thus, CPVT point mutations reveal significant mechanistic insight into RyR structure–function. There are >150 CPVT point mutations, mostly clustered within four distinct hot spots along the length of the RyR2 (Priori and Chen, 2011). Intriguingly, Thomas et al. (2007) suggested these hot spots are likely regions involved in RyR2 Ca^{2+} modulation and interdomain interactions (Yamamoto et al., 2000). They also

*A. Uehara, T. Murayama, M. Yasukochi, and N. Kurebayashi contributed equally to this paper.
Correspondence to Akira Uehara: ueharaak@fukuoka-u.ac.jp; or Nagomi Kurebayashi: nagomik@juntendo.ac.jp

Abbreviations used: CMV, cytomegalovirus; CPVT, catecholamine-induced polymorphic VT; IRES, internal ribosome entry site; RyR, ryanodine receptor; VSVG, vesicular stomatitis virus G protein; VT, ventricular tachycardia; WPRE, Woodchuck hepatitis virus posttranscriptional regulatory element.

The Rockefeller University Press $30.00
J. Gen. Physiol. 2017 Vol. 149 No. 2 199–218
https://doi.org/10.1085/jgp.201611624

suggested that the underlying mechanisms of RyR2 dysfunction are not uniform among CPVT mutants. However, only a small number of CPVT mutations have been functionally explored in heterologous expression studies (Jiang et al., 2002, 2004, 2005; Liu et al., 2013) or knock-in mice studies (Cerrone et al., 2005).

Here, we detail the function of a novel CPVT mutation in RyR2 (K4750Q, nucleotide change of a14251c in the *RyR2* gene; Kawamura et al., 2013). This mutation causes the most striking RyR2 dysfunction and CPVT phenotype known to date. The CPVT patient carrying RyR2-K4750Q experiences polymorphic tachycardia when just walking (Sugiyasu et al., 2009). We compare the function of this novel unusually severe RyR2 mutation with that of the well-studied RyR2-R2473S mutation (Jiang et al., 2005; Uchinoumi et al., 2010). RyR2-R2473S dysfunction is attributed to unzipping of the RyR2's N-terminal (1–600) and central domains (2,000–2,500), the domain switch hypothesis (Thomas et al., 2007).

We simultaneously measured WT and mutant RyR2 cytosolic and ER luminal Ca^{2+} signaling in HEK293 cells using novel genetically encoded non-FRET–based Ca^{2+} sensors. Specifically, these are G-GECO1.1 for Ca^{2+} in the cytosol (Zhao et al., 2011) and R-CEPIA1er Ca^{2+} sensor inside the ER (Suzuki et al., 2014). Results were informed by [^{3}H]ryanodine binding and RyR2 single-channel function measurements. We report that the K4750Q RyR2 point mutation caused multiple defects in single RyR2 function. The K4750Q mutation dramatically alters RyR2 gating kinetics and cytosolic and luminal Ca^{2+} sensitivity as well as abolishes cytosolic Ca^{2+}/Mg^{2+} inactivation. This extent of RyR2 functional defects is the greatest among all known CPVT-associated RyR2 point mutants, consistent with its severe human phenotype. Our findings indicate that the 4750 residue sits at a functionally critical point in the RyR2 channel structure.

MATERIALS AND METHODS

Materials

[^{3}H]Ryanodine and phospholipids were purchased from NEN Life Science Products and Avanti Polar Lipids, Inc., respectively. All other chemicals were of analytical grade.

Construction of expression plasmids

The coding sequence for mouse RyR2 (NM_023868.2) was amplified as five fragments (F1, 1–2,351; F2, 2,351–4,404; F3, 4,404–8,861; F4, 8,861–10,185; and F5, 10,185–14,901) by PCR using cDNA from mouse ventricle as the template. The PCR primers used are listed in Table S1. The fragments were cloned into the expression vector (pcDNA5/FRT/TO; Thermo Fisher Scientific). Construction of full-length RyR2 was performed by ligating these fragments using specific restriction enzymes.

Mutagenesis

The CPVT mutations, R2473S and K4750Q, were introduced by inverse PCR using F3 and F5 as the template, respectively. The mutations were confirmed by DNA sequencing.

Generation of stable inducible HEK293 cell lines

HEK293 cells stably and inducibly expressing WT or mutant RyR2s were generated using the Flp-In T-REx system (Thermo Fisher Scientific; Murayama et al., 2011). Clones with suitable expression of RyR2s were selected and used for experiments.

SDS-PAGE and Western blotting

SDS-PAGE was conducted on 3–15% linear gradient gel. 15-µg microsomes from HEK293 cells were applied to the gel. The separated proteins were electrophoretically transferred onto PVDF membranes. Western blotting was performed using antibodies for RyR2 (Chugun et al., 2003) and calnexin (C4731; Sigma-Aldrich). All of WT-, R2473S-, and K4750Q-expressing cells exhibited similar expression level of RyR2 proteins in ER membranes (Fig. S1 A).

Imaging of Ca^{2+} dynamics in the cytosol and ER in HEK293 cells expressing WT or mutant channels

Cytosolic-only Ca^{2+} measurements were performed on HEK293 cells expressing WT or mutant RyR2s grown on a glass-bottom dish for 26–30 h after induction by doxycycline. Note that these cells were not induced to express the RyR2's protein partners that are present in cardiac muscle cells. Thus, the results reflect solely RyR2 functional attributes. Experiments were performed at 26°C. For determination of cytoplasmic Ca^{2+} oscillations, HEK293 cells were loaded with 4 µM fluo-4 AM in culture medium for 30 min at 37°C and then incubated with Krebs solution (140 mM NaCl, 5 mM KCl, 2 mM $CaCl_2$, 1 mM $MgCl_2$, 11 mM glucose, and 5 mM HEPES, pH 7.4). The dish was placed on the stage of an inverted microscope equipped with the Nipkow disc confocal system (CSU22; Yokogawa Electric Corporation). Cells were at first treated with 10 mM caffeine to deplete Ca^{2+} and then equilibrated with normal Krebs solution for 10 min. Subsequently, fluo-4 signals, excited at 488 nm and emitting at 525 nm, were captured with an EM-CCD camera at 700-ms intervals (model 8509; Hamamatsu Photonics). At the end of each experiment, high Ca^{2+} Krebs solution containing 20 mM Ca^{2+} and 20 µM ionomycin was applied to obtain maximal fluorescence intensity (F_{max}) of fluo-4 in individual cells. Mean fluorescence intensities in individual cells were determined using region of interest (ROI) analysis with AquaCosmos software (Hamamatsu Photonics) and normalized to the F_{max}.

For simultaneous recording of ER luminal Ca^{2+} ($[Ca^{2+}]_{lum}$) and cytosolic Ca^{2+} ($[Ca^{2+}]_{cyt}$), cells were cotransfected with a pair of genetically encoded Ca^{2+} sensor proteins. pCMV R-CEPIA1er (Addgene plasmid #58216; a gift from M. Iino, University of Tokyo, Tokyo, Japan) and CMV G-GECO1.1 (Addgene plasmid #32445; a gift from R. Campbell, University of Alberta, Edmonton, Alberta, Canada) were used for the measurements of $[Ca^{2+}]_{lum}$ and $[Ca^{2+}]_{cyt}$, respectively. Doxycycline was added to the culture medium at the time of transfection. At 26–30 h after transfection, cells were washed with Krebs solution and placed on the stage of the microscope. G-GECO1.1 (Zhao et al., 2011) and R-CEPIA1er (Suzuki et al., 2014) were excited by 488- and 568-nm laser light, respectively, and fluorescence images at 525 and 620 nm were simultaneously captured, side-by-side on the same camera, using the W-view system (Hamamatsu Photonics). In a typical series of Ca^{2+} measurements, both cytoplasmic and ER Ca^{2+} signals were sequentially recorded as follows (see Fig. 5): (a) Ca^{2+} oscillations were monitored in normal Krebs solution for 8 min. (b) 10 mM caffeine was applied to deplete Ca^{2+} from ER. (c) After washing with Ca^{2+}-free Krebs solution (~10 s), cells were treated with 20 µM ionomycin and 3 mM BAPTA in Ca^{2+}-free Krebs solution to obtain minimal fluorescence level (F_{min}) for 2 min. (d) Finally, cells were treated with 20 mM Ca^{2+} and 20 µM ionomycin to obtain F_{max}. $[Ca^{2+}]_{lum}$ was calculated using parameters obtained by in situ titration according to Suzuki et al. (2014).

Expression of RyR2 and G-GECO1.1 in HL-1 cardiac cells and Ca^{2+} imaging

HL-1 cardiac cells derived from mouse atrial cardiac muscle cells (Claycomb et al., 1998) were provided by M. Yamada (Shinshu University, Matsumoto, Japan), after obtaining the approval of W.C. Claycomb (Louisiana State University Health Sciences Center, New Orleans, LA). HL-1 cells were maintained in fibronectin/gelatin-precoated flasks in the supplemented Claycomb medium (JRH Biosciences) containing 10% fetal bovine serum, 100 U/ml penicillin/100 µg/ml streptomycin, 2 mM glutamine, and 0.1 mM norepinephrine as described previously (Claycomb et al., 1998). Recombinant WT or mutant RyR2 was expressed using baculovirus expression system (see next section). For Ca^{2+} imaging of nonbeating HL-1 cells (Fig. S2), cells were grown on a 35-mm glass-bottom dish at low density and were incubated with the purified baculovirus solution of RyR2-IRES-mCherry and G-GECO1.1 in a serum-free Claycomb medium for 4 h at 37°C in a CO_2 incubator. After infection, HL-1 cells were cultured in the supplemented Claycomb medium for 48 h. G-GECO1.1 signals were monitored in cells showing mCherry signals (488-nm excitation/525-nm emission, frame rate: 25/s). Ca^{2+} measurements were performed at 30°C. For $[Ca^{2+}]_{cyt}$ imaging of beating HL-1 (Fig. 4), near-confluent HL-1 cells were infected with RyR2-IRES-mCherry baculovirus. The Ca^{2+} imaging was performed 24 h after infection using Cal520-AM (AAT Bioquest).

Production of baculovirus

Baculovirus that effectively infects mammalian cells was obtained by expressing vesicular stomatitis virus G protein (VSVG) on the virus envelope (Tani et al., 2001). The virus was produced by Bac-to-Bac system (Invitrogen) using the modified donor vector (pFastBac1-VSVG-CMV-WPRE) that was constructed as follows. Cytomegalovirus (CMV) promoter was amplified by PCR with primers (5′-AAGGATCCTAGTTATTAA TAGTAATCAAT-3′ and 5′-CCGAATTCTTGGAAGCTT TAGCGCTAGCGGATCTGACGG-3′) using pEGFP-N1 (Takara Bio Inc.) as a template, digested by BamHI–EcoRI and ligated with pFastBac1 (Invitrogen) in which existing HindIII and EcoRV sites have been deleted. Woodchuck hepatitis virus posttranscriptional regulatory element (WPRE) was PCR amplified from pWPT-GFP (Addgene plasmid #12255; gift from D. Trono, École Polytechnique Fédérale de Lausanne, Lausanne, Switzerland) with primers (5′-GGCTCG AGAATTGATATCTCAACCTCTGGATTACAAAAT-3′ and 5′-TTGGTACCAATTCCCGATGCGGGGAGGCG-3′), digested by XhoI–KpnI and ligated with the above vector. Coding sequence for VSVG and following SV40 polyadenylation signal sequence was amplified with primers (5′-CCGGATCCATGAAGTGCCTTTTGTAC TTA-3′ and 5′-CCGAATTCAATTCGTACGCGGATC TCCTAGGCTCAAGCA-3′) from pFBG-CAG (Tani et al., 2001), digested by BamHI–BsiWI and inserted into downstream of polyhedrin promoter of the above vector to yield the final pFastBac1-VSVG-CMV-WPRE vector.

Construction of donor vector for G-GECO1.1 and RyR2-IRES-mCherry was as follows. cDNA for G-GECO1.1 was PCR amplified from CMV-G-GECO1.1 (Addgene plasmid #32445; a gift from R. Campbell) and inserted in pFastBac1-VSVG-CMV-WPRE to obtain the pFastBac1-VSVG-G-GECO1.1 vector. The internal ribosome entry site (IRES) from pIRES-EGFP (Takara Bio Inc.) and mCherry (Shaner et al., 2004) coding sequence (gift from R.W. Tsien, University of California, San Diego, La Jolla, CA) was ligated in tandem, PCR amplified, and inserted in the pFastBac1-VSVG-CMV-WPRE vector. cDNA for full-length WT or mutant RyR2 was excised from the pcDNA5-FRT-TO-RyR2 vector and inserted into the above vector to yield the pFastBac1-VSVG-RyR2-IRES-mCherry vector.

Baculovirus was produced in Sf9 cells according to the manufacturer's instructions (Invitrogen). The virus was purified by sucrose density gradient ultracentrifugation (Tani et al., 2001), resuspended in phosphate-buffered saline, and stored at 4°C until used.

[^{3}H]Ryanodine binding

Ryanodine binds to the open RyR channel, and thus, [^{3}H]ryanodine binding is often used to access RyR channel regulatory attributes. HEK293 cell microsomes were prepared by nitrogen cavitation (Murayama et al., 2011). Microsomes (50–100 µg of protein) were incubated with 5 nM [^{3}H]ryanodine for 1 h at 25°C in a 100-µl solution containing 0.17 M KCl, 20 mM MOP SO, pH 7.0, and various concentrations of free Ca^{2+}. The protein-bound [^{3}H]ryanodine was separated by filtering through polyethyleneimine-treated glass filters (Whatman GF/B). Nonspecific binding was determined in the presence of 20 µM unlabeled ryanodine. The [^{3}H]ryanodine binding data (B) were normalized to the maximal binding for [^{3}H]ryanodine (B_{max}), which was separately determined by Scatchard plot analysis using varied concentrations of [^{3}H]ryanodine (3–20 nM) in the medium containing 1 M NaCl. The resultant B/B_{max} represents an averaged activity of individual channels and thereby compares quantitatively between WT and mutants.

Purification of RyR2 by sucrose gradients

HEK293 cell microsomes (from five 150-mm dishes) were solubilized for 30 min on ice in buffer A (0.3 M NaCl, 20 mM Tris-HCl, pH 7.5, 2 mM dithiothreitol, and a cocktail of protease inhibitors) supplemented with 1% CHAPS, 0.5% soybean lecithin. After ultracentrifugation (100,000 *g*, 30 min at 4°C), the supernatant was applied onto a 5–30% sucrose gradients in a buffer supplemented with 0.3% CHAPS and 0.15% soybean lecithin. Gradients were centrifuged for 18 h at 25,000 rpm at 4°C using Hitachi P40ST rotor. Resulting fractions (700 µl each) were analyzed for SDS-PAGE. Peak fractions containing RyR2s were combined, divided into aliquots, quickly frozen in liquid nitrogen, and stored at −80°C before use. A typical SDS-PAGE pattern of sucrose gradients is shown in Fig. S1 B.

Single-channel recording

Purified RyR2 channels were isolated from HEK293 cells expressing the recombinant protein. Single-channel currents were measured according to the conventional planar lipid bilayer technique described elsewhere (Lindsay et al., 1991; Uehara et al., 1996; Guo et al., 2012). In brief, single channels were recorded in a symmetrical 250 mM KCl solution and 20 mM HEPES, pH 7.4. The cis side of the bilayer was virtually grounded. The cis chamber corresponds to the cytosolic face of the channel. Electrical signals were low-pass filtered at 1–5 KHz and digitized at 10–40 KHz. All experiments were performed at room temperature. Single-channel analysis was performed using pClmap10 software (Molecular Devices), and Po determinations were made from current recordings lasting >3 min.

Kinetic analysis of single-channel data

The state models of WT and mutant RyR2 were constructed with QuB software for the gating kinetics of single molecules (Nicolai and Sachs, 2013) according to Mukherjee et al. (2012). In brief, the single-channel currents of a few minutes were idealized using an Idl/Base function in which the interactive hidden Markov model-based maximization algorithm is used. A dead time of 0.179 ms was imposed during idealization. The open and closed time histograms generated by the initial idealization were fitted with a mixture of exponential probability density functions with a maximum interval likelihood function. The continuous time likelihood of a dwell time sequence was maximized first-order correction of missed events (Qin et al., 1996). The program finds the most likely rate constants, given a connection scheme and the channel data. A closed or an open state was added to the initial kinetic model, until the fitting of the probability distribution function was appropriate and any further additions did not alter the maximum likelihood value significantly. The absolute value of the maximum log likelihood at convergence was finally obtained by increasing with every significant addition of dwelling state to sequence. Moreover, the state models with their respective estimated rates of transitions were used for stochastic simulation of single-channel data. To get the validity of each model, we confirmed whether the gating behavior of the model-based simulated traces appears to be similar to that of the original traces obtained from experiments.

Determination of free Ca^{2+} concentration

Free Ca^{2+} concentrations of solutions were calculated by WebMAXC program (Stanford University) and verified using a Ca^{2+}-selective electrode.

Hill fitting

Ca^{2+}-dependent [^{3}H]ryanodine binding and single-channel Po data were fitted to the following equation:

$$A = A_{max} \times \left(\left[Ca^{2+}\right]^{nA} / \left(\left[Ca^{2+}\right]^{nA} + K_A{}^{nA} \right) \right) / \left(1 - \left[Ca^{2+}\right]^{nI} / \left(\left[Ca^{2+}\right]^{nI} + K_I{}^{nI} \right) \right), \quad (1)$$

where K_A and K_I are dissociation constants, and nA and nI are Hill coefficients for activation and inactivation, respectively. In addition, A is the activity at the specified Ca^{2+} and A_{max} is the gain that scales the maximal attainable activity (Murayama and Kurebayashi, 2011).

Statistics

All values shown are mean ± SEM. Unless otherwise stated, Student's *t* test was used to compare two groups. P-values <0.05 were considered significant.

Online supplemental material

Fig. S1 shows heterologous expression and isolation of recombinant RyR2 proteins. Fig. S2 shows G-GECO1.1

Ca^{2+} signals in nonbeating cardiac HL-1 cells expressing WT and mutant RyR2s. Fig. S3 shows confocal Ca^{2+} imaging on RyR2-expressing HEK293 cells. Fig. S4 shows the effects of tetracaine on ER Ca^{2+} signals obtained with R-CEPIA1er in HEK293 cells expressing WT or mutant RyR2s. Fig. S5 shows the effects of RyR2 expression level on Ca^{2+} homeostasis in HEK293 cells. Fig. S6 shows dose-dependent [^{3}H]ryanodine binding to WT and mutant RyR2 channels. Fig. S7 shows Mg^{2+} action on Ca^{2+}-dependent [^{3}H]ryanodine binding. Fig. S8 shows sensitivities of our single-channel currents to various RyR2 ligands. Fig. S9 shows open and closed time histograms with exponential fittings to construct state models and simulated currents. Fig. S10 shows state models and simulated currents focusing on $[Ca^{2+}]_{cyt}$-dependent inactivation. Video 1 shows cytoplasmic Ca^{2+} signals in control HL-1 cells expressing no recombinant RyR2. Video 2 shows cytoplasmic Ca^{2+} signals in HL-1 cells expressing RyR2-WT. Video 3 shows cytoplasmic Ca^{2+} signals in HL-1 cells expressing RyR2-K4750Q. Video 4 shows cytoplasmic and ER-luminal Ca^{2+} signals in HEK293 cells expressing RyR2-WT. Table S1 lists forward and reverse primers used for construction of full-length RyR2. Table S2 shows time constants and relative areas for exponential fits of closed and open time distributions.

RESULTS

Proband carrying a de novo RyR2-K4750Q showed the severe phenotype

A de novo RyR2-K4750Q mutation was identified in a 14-yr-old girl, and this allele was heterozygous (Fig. 1 A; Sugiyasu et al., 2009; Kawamura et al., 2013). She had no other CPVT-linked mutation in RyR2, CASQ2, CALM1, TRND, or KCNJ2 (not depicted). At the age of 6 yr, she began to experience repeated exercise-induced syncope caused by sustained polymorphic VT, which was treated by exercise avoidance, propranolol, and digoxin. Atrial fibrillation was also noted and likely caused by RyR2-K4750Q dysfunction in the atria. When 13 yr old, the patient underwent catheter ablation therapy, and multifocal atrial tachycardia mimicking atrial fibrillation was found to originate from multiple pulmonary venous foci. After pulmonary venous isolation, sustained polymorphic VT appeared during routine exercise like walking upstairs or straining to defecate (Fig. 1 B). In our CPVT patient cohort, she was among one of the youngest in onset and severest of phenotypes. Her echocardiogram showed normal cardiac function and no structural heart disease.

RyR2-K4750Q mutation loci

The K4750 residue is well conserved across animal species and RyR1-3 isoforms, implying that this residue may be essential for normal RyR2 function (Fig. 2 A). Several distinct RyR1/2 topology models (Welch et al., 2004; Ramachandran et al., 2013; Chen et al., 2014; Yan et al., 2015) have been reported to date. We adopt the newest topology model of Yan et al. (2015), in which the K4750 residue is located between S4 segment and S4–5 linker. Intriguingly, our homology RyR2 modeling of the transmembrane region (Fig. 2 B) indicates that the K4750 residue faces the cytosol just outside the pore domain, suggesting a role for this residue in regulating pore gating. In contrast, the well-studied RyR2-R2473S CPVT-linked mutation occurs on the cytoplasmic side of the channel but within the zipper domain, which is far from the K4750Q locus and pore domain (Fig. 2 C).

Mutant RyR2-mediated Ca^{2+} handling in cells

We generated HEK293 cells that stably and inducibly express RyR2-WT, -R2473S, or -K4750Q. Ca^{2+} measurements were performed 26–30 h after induction by doxy cycline. The HEK293 cells expressed similar levels of the full-length RyR2 protein (Fig. S1 A). Cells harboring WT, R2473S, and K4750Q RyR2s were loaded with fluo-4 AM, and single-cell cytosolic Ca^{2+} signals were obtained (Fig. 3 A). Spontaneous cytosolic Ca^{2+} oscillations were observed as reported previously by Chen and his colleagues (Jiang et al., 2002, 2004, 2005). As in their studies, the spontaneous Ca^{2+} oscillations were monitored as extracellular Ca^{2+} level ($[Ca^{2+}]_o$) was gradually elevated. At the end of each measurement, 20 µM ionomycin and 20 mM extracellular Ca^{2+} were applied to the cells to obtain maximal fluorescence intensity of Ca^{2+}-bound fluo-4 (F_{max}) in individual cells. As shown in Fig. 3 A (top and bottom left), Ca^{2+} oscillations occurred at lower $[Ca^{2+}]_o$ in cells expressing R2473S and K4750Q, compared with WT. The percentage of WT cells having spontaneous Ca^{2+} oscillations increased as a function of extracellular Ca^{2+} (Fig. 3 A, bottom right). This relationship was shifted in R2473S cells and even more so in K4750Q cells. The frequency and amplitude of the Ca^{2+} oscillations were quantified at 2 mM $[Ca^{2+}]_o$ (Fig. 3 B). Cells harboring mutant RyR2s had significantly more frequent and smaller amplitude Ca^{2+} oscillations as well as higher resting (between oscillation) Ca^{2+} levels, compared with WT. The change in each of these parameters was more severe in K4750Q cells than in R2473S cells.

To characterize the channel properties in a cellular context close to that of cardiac myocytes, analogous Ca^{2+} oscillation studies were performed in the cardiac HL-1 cells (Claycomb et al., 1998) to reproduce in cellular milieu of cardiac myocytes. Recombinant RyR2s were expressed by the baculovirus system, as it is more suitable for transduction of such large DNA in mammalian cells (Tani et al., 2001). mCherry (Shaner et al., 2004) was used as a reporter of transduction and Ca^{2+} signals were monitored with G-GECO1.1 (Zhao et al., 2011).

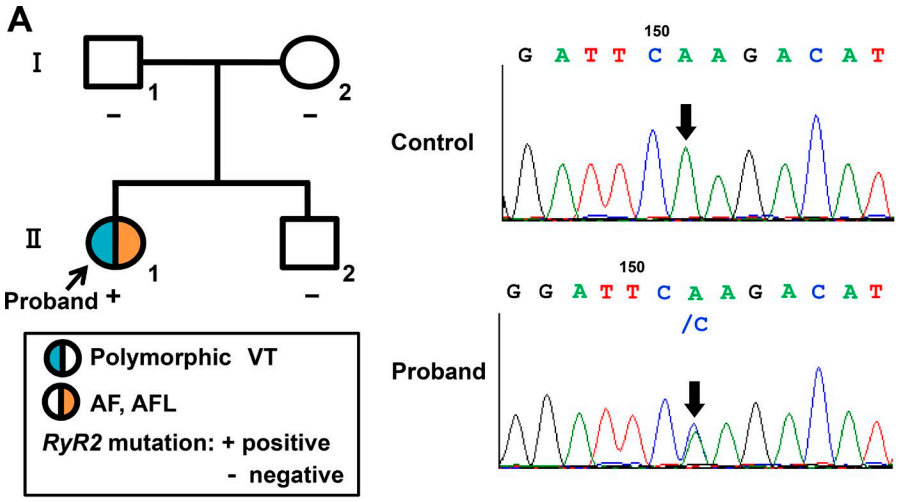

Figure 1. **Genotype and phenotype of a female patient carrying the CPVT-associated RyR2 mutation of c.14251A>C (K4750Q).** (A) Genetic testing. Family pedigree (left) and genotyping of the proband (right). Holter ECG monitored with leads CC5 and mV1. (B) ECG monitoring. This patient exhibited atrial tachycardia (top, see P waves on right half recording) and subsequent VT (bottom, entire record) while walking upstairs.

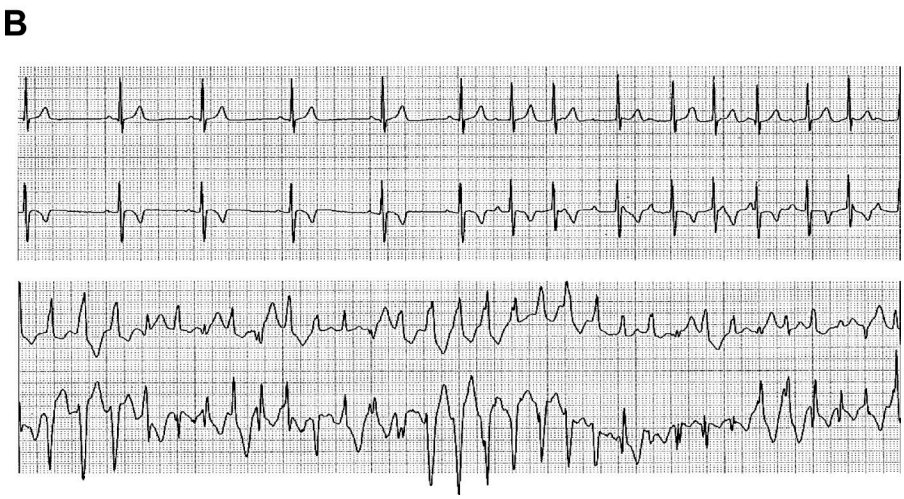

After 48 h of baculovirus infection, G-GECO1.1 signals in HL-1 cells showing mCherry fluorescence were recorded. For this measurement, semiconfluent HL-1 cells that did not display spontaneous beating were chosen. The resulting RyR2-mediated oscillation in HL-1 cells occurred at higher frequency than in HEK293 cells. Like the HEK293 cells, however, HL-1 cells harboring the K4750Q mutant had more frequent Ca^{2+} oscillations than WT or R2473S HL-1 cells (Fig. S2). Qualitative assessment of SR Ca^{2+} load conducted in HL-1 cells using peak caffeine-evoked Ca^{2+} release as shown in Fig. S2 suggests that cardiac cells expressing RyR2-K4750Q mutants have lower SR Ca^{2+} content than cells expressing RyR2-WT.

Subsequently, Ca^{2+} measurements were made in the beating confluent HL-1 cells. Ca^{2+} signals were monitored with the Ca^{2+} indicator (Cal520) 24 h after baculovirus infection. Although HL-1 cells did not respond to electrical field stimulation, clustered cells displayed spontaneous, highly rhythmic, and synchronized Ca^{2+} transients. This synchrony was probably paced by autogenic action potentials in one of the clustered cells. We analyzed Ca^{2+} signals within such clusters of HL-1 cells that were expressing exogenous RyR2s (Fig. 4). Control beating clusters of HL-1 cells that had not undergone baculovirus infection rarely displayed Ca^{2+} waves (Video 1 and Fig. 4, B [d] and D [d]). The expression of exogenous WT RyR2 induced occasional Ca^{2+} waves (Video 2 and Fig. 4, A [left] and B [c]) in 13 out of 28 mCherry-positive cells during the 50-s measurement window. However, clustered beating HL-1 cells harboring the K4750Q mutant showed frequent Ca^{2+} waves that occurred shortly after the cell- and cluster-wide Ca^{2+} transients (Video 3 and Fig. 4, C [left] and D [b and c]) in 17 out of 25 cells. Ca^{2+} wave frequency in the K4750Q cells was significantly higher than that in WT cells (Fig. 4 E). Addition of 1 µM isoproterenol did not substantially change frequency of cell-wide Ca^{2+} transients or spontaneous Ca^{2+} waves. This is likely because HL-1 cells were maintained in the Claycomb culture medium, which contains 100 µM norepinephrine. However, Ca^{2+} waves were more frequent when the $[Ca^{2+}]_{lum}$ was elevated by bathing the cells in high $[Ca^{2+}]_o$ (Fig. 4 F). These results indicate that the K4750Q mu-

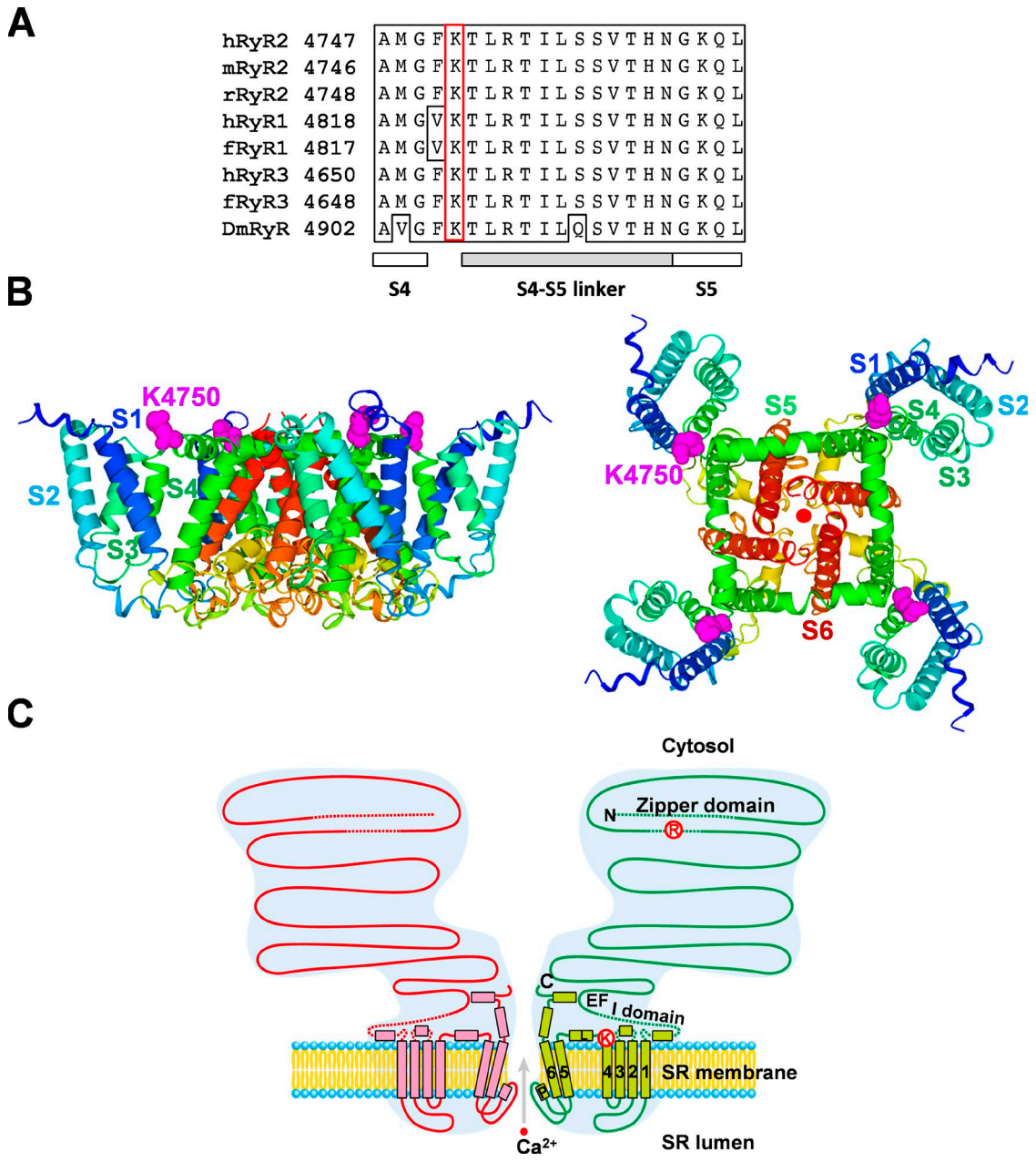

Figure 2. **CPVT-associated mutation loci in a RyR2 channel molecule.** (A) Alignment of the sequences around S4–5 linker of RyR orthologues. Letters h, m, r, f, and Dm represent human, mouse, rabbit, frog, and *D. melanogaster* (fruit fly), respectively. (B) The mutation locus of K4750Q in a homology model of the RyR2 channel domain. (left) View of tetramers parallel to the plane of the lipid bilayer membrane. (right) View of tetramers from the cytosol. Magenta balls, K4750 residues; reddish brown ribbons, S6 segments (helices); yellowish green ribbons, S5 segments (helices); red ball, Ca^{2+}. (C) The mutation sites of R2473S and K4750Q in the full-length RyR2 depicted by the letters R and K, respectively. Zipper domains, I domain, and EF hands for the putative Ca^{2+} binding sites are also illustrated.

tant increases Ca^{2+} wave propensity in cardiac-like cellular milieu and that wave frequency increases in Ca^{2+} overload conditions.

The cytosolic ($[Ca^{2+}]_{cyt}$) and intra-ER Ca^{2+} ($[Ca^{2+}]_{lum}$) signals in RyR2-expressing HEK293 cells were simultaneously measured using G-GECO1.1 and R-CEPIA1er, respectively (Video 4 or Fig. S3 and Fig. 5; Suzuki et al., 2014; Murayama et al., 2015). Spontaneous oscillations of $[Ca^{2+}]_{cyt}$ and $[Ca^{2+}]_{lum}$ occurred in WT, R2473S, and K4750Q cells (Fig. 5 A). The R-CEPIA1er signal is not an exact mirror image of the G-GECO1.1 signal. The G-GECO1.1 signal returned to their resting level faster than R-CEPIA1er signal. Before the spontaneous Ca^{2+} release events, $[Ca^{2+}]_{lum}$ reached a maximum (threshold level 1; Fig. 5 A, bottom left), and this corresponds to the RyR2 $[Ca^{2+}]_{lum}$ activation threshold. The mini-

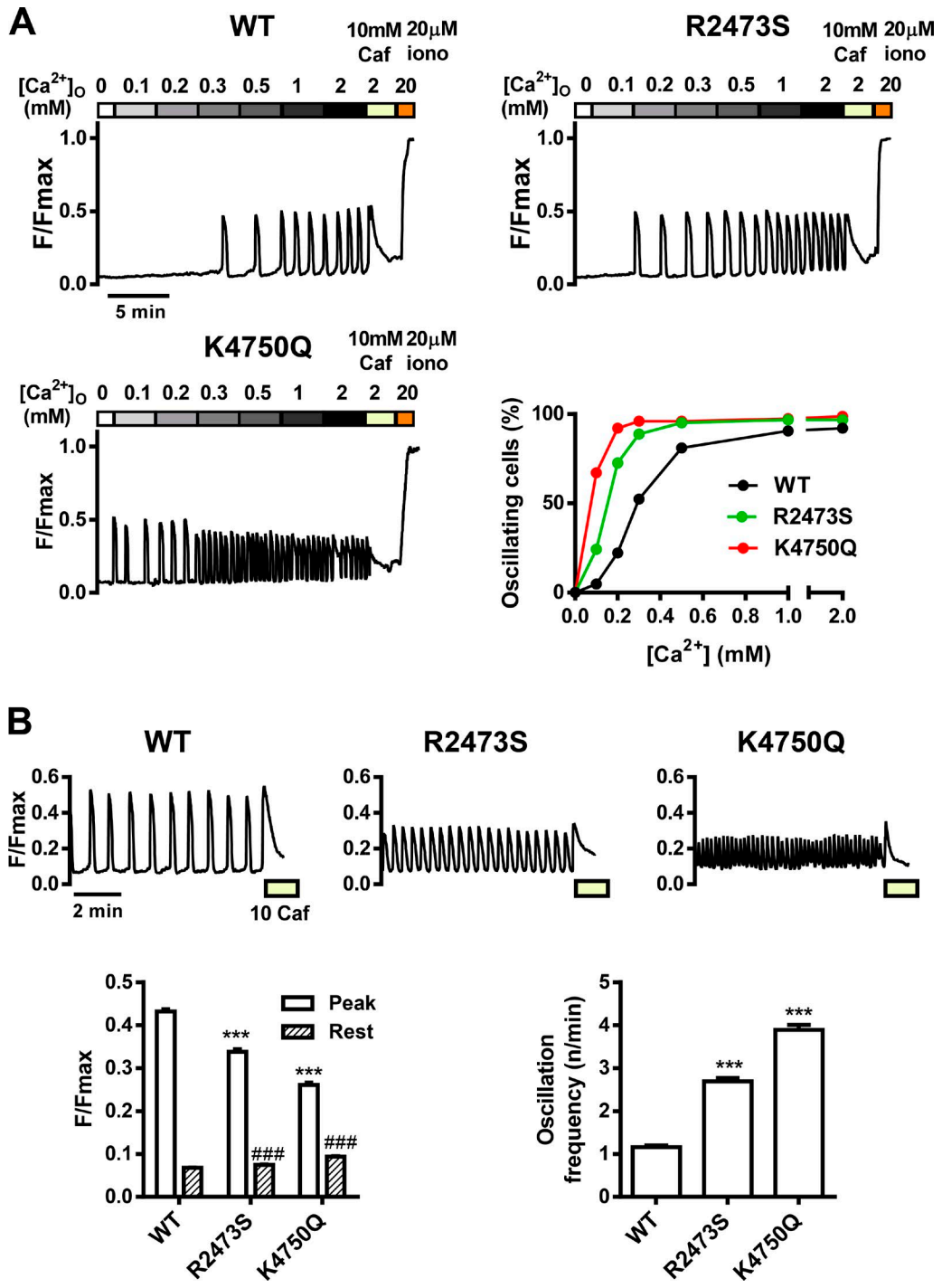

Figure 3. **Cytoplasmic Ca^{2+} signals in RyR2-WT, -R2473S, and -K4750Q expressing HEK293 cells.** (A) Representative fluo-4 signals of WT and mutant cells at various $[Ca^{2+}]_o$ (top and bottom left). (bottom right) Fraction of cells showing Ca^{2+} oscillations. (B) Comparison of oscillations at 2 mM $[Ca^{2+}]_o$ among WT and mutant cells. (top) Representative fluorescence signals. (bottom left) Oscillation amplitude (F/F_{max}) at peak and rest. ***, $P < 0.001$ versus WT peak. ###, $P < 0.001$ versus WT rest. (bottom right) Oscillation frequency (*n*/min). $n = 182$, 181, and 146 for WT, R2473S, and K4750Q, respectively. ***, $P < 0.001$ versus WT. Values shown are mean ± SEM.

mal level of $[Ca^{2+}]_{lum}$ resulting from the spontaneous Ca^{2+} release events (threshold level 2; Fig. 5 A) corresponds to the RyR2 $[Ca^{2+}]_{lum}$ termination threshold. Both threshold level 1 and 2 were reduced in R2473S or K4750Q cells compared with WT cells. Our quantification of the R-CEPIA1er signal (K_d, n, F_{max}, and F_{min}) permitted calculation of $[Ca^{2+}]_{lum}$ at thresholds 1 and 2 in WT, R2473S, and K4750Q cells (Fig. 5 B). In WT

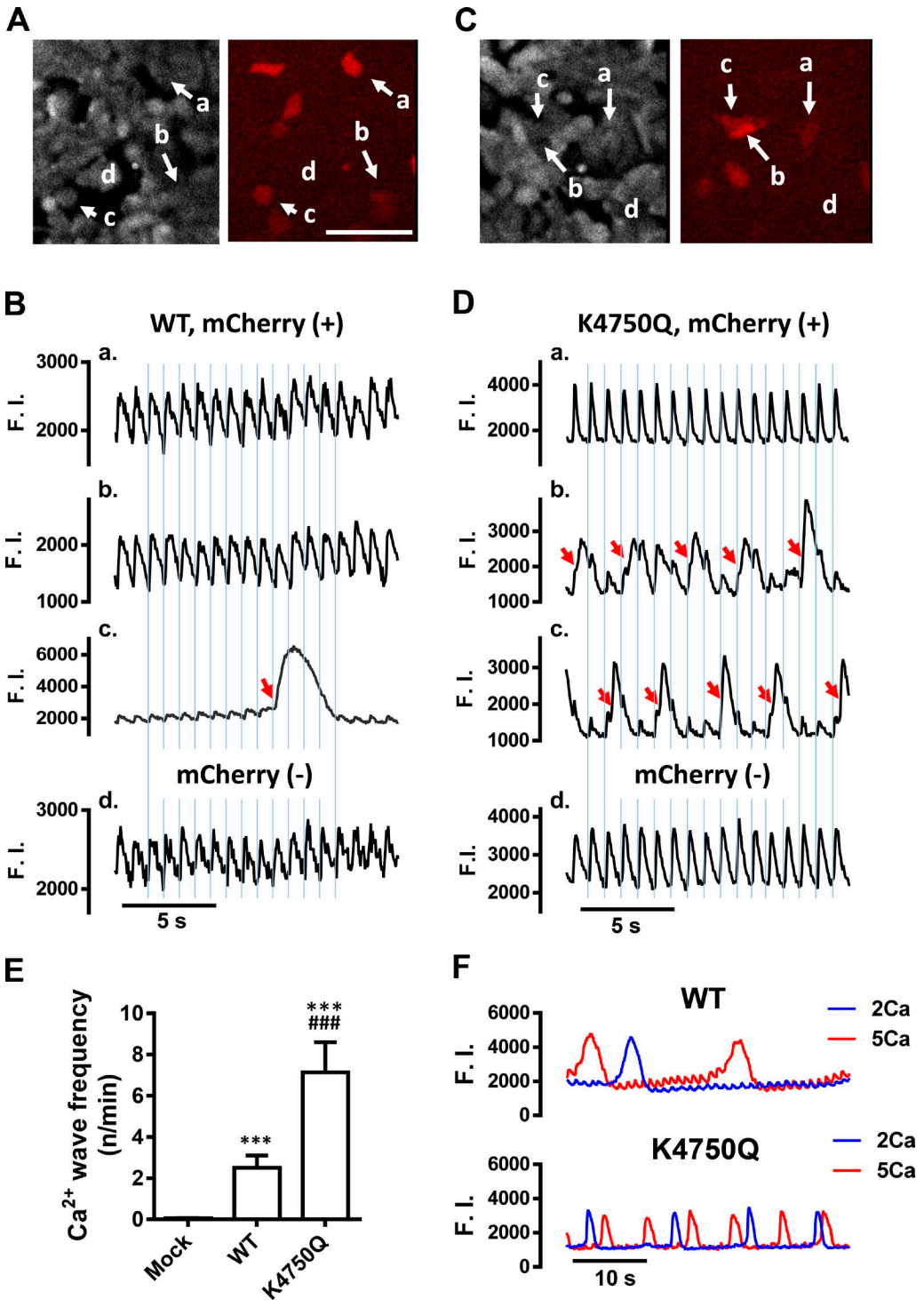

Figure 4. **Cytoplasmic Ca^{2+} signals in beating HL-1 cardiomyocytes expressing exogenous RyR2-WT and -K4750Q.** (A) Cal520 (left) and mCherry (right) fluorescent images of HL-1 cells infected with WT-IRES-mCherry baculovirus. Bar, 100 µm. (B) Representative Ca^{2+} signals in mCherry-positive (a–c) and mCherry-negative cells (d). Thin blue lines indicate the onset of synchronized Ca^{2+} transients (a–d), induced by autogenic within clusters of HL-1 cells. The red arrow depicts the onset of a Ca^{2+} wave (c). Cells (a and b) displayed normal Ca^{2+} transients but no Ca^{2+} waves. (C) Cal520 (left) and mCherry (right) fluorescent images of HL-1 cells infected with K4750Q-IRES-mCherry baculovirus. (D) Representative Ca^{2+} signals in mCherry-positive (a–c) and mCherry-negative cells (d). Note that single Ca^{2+} waves (red arrows) occurred every three to four Ca^{2+} transients (blue lines), and the peak amplitudes of the Ca^{2+} waves are larger than those of the synchronized Ca^{2+} transients. The cell (a) displayed normal Ca^{2+} transients but no Ca^{2+} waves. (E) Mean Ca^{2+} wave frequency in mock-infected and RyR2-WT and -K4750Q–expressing cells (n = 24–30). ***, $P < 0.001$ versus mock. ###, $P < 0.001$ versus WT. Values shown are mean ± SEM. (F) Typical Ca^{2+} signals at 2 mM (blue) and 5 mM (red) $[Ca^{2+}]_o$. Note that the Ca^{2+} wave frequency was higher at 5 mM than at 2 mM $[Ca^{2+}]_o$ in both WT and K4750Q cells.

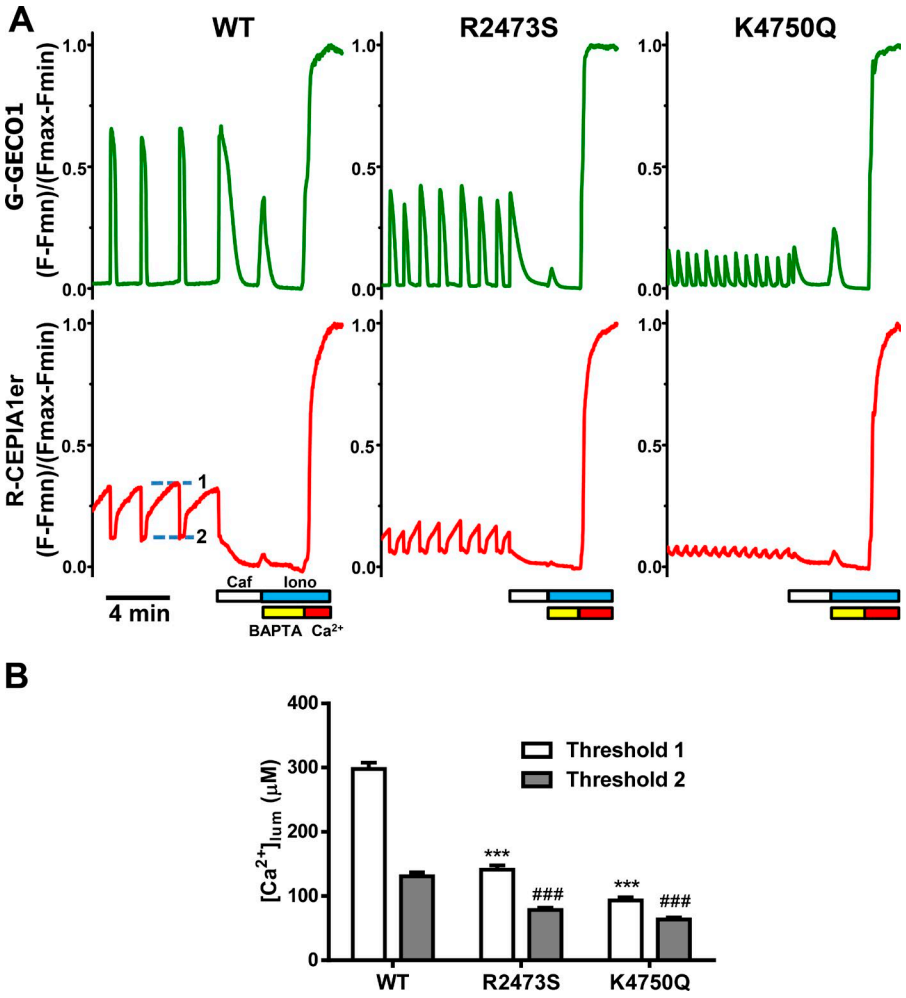

Figure 5. **Simultaneous cytosolic and ER Ca^{2+} monitoring in WT or mutant cells.** (A) Cytosolic and ER Ca^{2+} signals were monitored with G-GECO1.1 (top) and R-CEPIA1er (bottom), respectively. Representative fluorescence signals in WT (left), R2473S (middle), and K4750Q (right) cells. The numbers 1 and 2 near the left bottom trace mark luminal Ca^{2+} thresholds 1 and 2. (B) Bar graph comparing luminal Ca^{2+} threshold 1 and 2 in WT, R2473S, and K4750Q cells. n = 155 (WT), 122 (R2473S), and 107 (K4750Q). ***, $P < 0.001$ versus WT threshold 1. ###, $P < 0.001$ versus WT threshold 2. Values shown are mean ± SEM.

cells, the $[Ca^{2+}]_{lum}$ at which spontaneous Ca^{2+} release occurred (threshold 1) was ∼300 µM. This was substantially lower than the $[Ca^{2+}]_{lum}$ of control cells expressing no RyR2s (568 ± 18 µM, n = 55), indicating that the expression of WT RyR2 lowers $[Ca^{2+}]_{lum}$ by introducing an additional ER Ca^{2+} leak pathway. Threshold 1 in R2473S and K4750Q cells was ∼140 µM and ∼95 µM, respectively. Although mutants significantly reduced RyR2 $[Ca^{2+}]_{lum}$ activation threshold, the reduction caused by the K4750Q mutation was substantially greater. Releasable Ca^{2+} can be calculated as the difference between thresholds 1 and 2. Releasable Ca^{2+} was smaller in R2473S and K4750Q cells, explaining the smaller cytoplasmic Ca^{2+} transients compared with those in WT cells (Figs. 3 and 5 A). The dramatic drop in ER Ca^{2+} stores in K4750Q cells is mostly likely caused by an abundance of ER Ca^{2+} leak. This interpretation is consistent with the observation that tetracaine (an RyR inhibitor) elevates $[Ca^{2+}]_{lum}$ in R2473S and K4750Q cells to levels close to those observed in WT cells (Fig. S4).

The aforementioned results demonstrate that $[Ca^{2+}]_{lum}$ in K4750Q cells is low compared with WT and R2473S HEK293 cells, and this is likely not the case in the patient. The markedly low $[Ca^{2+}]_{lum}$ in HEK293 cells is probably explained by mutant RyR2 overexpression. We therefore examined how expression levels of RyR2 influences cellular Ca^{2+} homeostasis. We determined the time course of $[Ca^{2+}]_{lum}$ as a function of time after induction (Fig. S5 A) as RyR2 protein levels increased over this period (Murayama et al., 2016). In WT RyR2–transfected cells, $[Ca^{2+}]_{lum}$ gradually decreased with time until 24 h (Fig. S5 A). In the mutant cells, $[Ca^{2+}]_{lum}$ decreased faster but also reached a steady-state at 24 h. At 4 h after induction, K4750Q-expressing cells still had a substantial $[Ca^{2+}]_{lum}$ and displayed clear Ca^{2+} oscillations (Fig. S5 B). The oscillation frequency of K4750Q was higher compared with 4-h post-induction WT and R2473S cells (Fig. S5 C). At 2 h after induction, Ca^{2+} oscillation frequency was high in K4750Q cells, but $[Ca^{2+}]_{lum}$ was similar to that in WT cells (Fig. S5 C, inset). These results suggest that HEK293 cell $[Ca^{2+}]_{lum}$ decreases with RyR2 expression level and that the K4750Q mutation increases Ca^{2+} oscillation frequency even at very low expression levels.

[^{3}H]Ryanodine binding

[^{3}H]Ryanodine binding reports RyR functional status (Chu et al., 1990; Murayama et al., 2000). The WT, 2473S, and K4750Q RyR2s had similar ryanodine K_d's (Fig. S6), thus indicating that affinity of ryanodine is not changed by these mutations. Therefore, [^{3}H]ryanodine binding likely reflects WT, 2473S, or K4750Q RyR2 functional status equally well. The Ca^{2+} dependence of ryanodine binding is shown in Fig. 6. In the absence of Mg^{2+} (Fig. 6 A), WT had the expected bell-shaped Ca^{2+} dependence with Ca^{2+} activation and inactivation phases. In contrast, binding in R2473S and K4750Q was enhanced over the whole Ca^{2+} range tested. With millimolar Mg^{2+} present (Fig. 6 B), the bell-shaped WT binding curve decreased in amplitude with its cytosolic Ca^{2+} activation phase significantly shifted rightward (Fig. S7 A). The presence of Mg^{2+} greatly increased the degree of binding to R2473S and K4750Q channels with an enhanced cooperativity of their cytosolic Ca^{2+} activation phase (Fig. S7, B and C). The increased binding with Mg^{2+} present is likely caused by the activation of Mg^{2+} regulatory sites, as reported elsewhere (Chugun et al., 2007; Gomez and Yamaguchi, 2014).

The [^{3}H]ryanodine binding in Fig. 6 B was fitted with a "double Hill" equation (Murayama and Kurebayashi, 2011; Eq. 1 in Materials and methods). Maximum binding (A_{max}) was threefold greater in R2473S (0.22 ± 0.03) and K4750Q (0.24 ± 0.05) than WT (0.08 ± 0.01). The Ca^{2+} activation EC_{50} was significantly lower in both R2473S (8.2 ± 0.7 µM) and K4750Q (6.9 ± 0.7 µM) compared with WT (16.5 ± 3.0 µM). The Ca^{2+} inactivation IC_{50} was increased in R2473S (6.5 ± 1.0 mM) compared with WT (2.4 ± 0.7 mM) and almost abolished in K4750Q (89 ± 6 mM). Ca^{2+} as well as Mg^{2+} binds to and acts at the RyR's cytosolic inactivation site (Laver et al., 1997a; Murayama et al., 2000). The Mg^{2+} dose dependence of binding at pCa 4 is shown in Fig. 6 C. Binding to both mutants initially increased with Mg^{2+} concentration almost equally, but at high Mg^{2+} levels, R2473S binding decreased substantially. High Mg^{2+} levels had much less effect on K4750Q binding. These results show that regulation of ryanodine binding (i.e., RyR functional status) by high divalent cation concentrations (Chu et al., 1990; Murayama et al., 2000) is nearly absent in the K4750Q mutant.

Single RyR2 channel recording

For single-channel recording, recombinant RyR2 proteins were purified from CHAPS-solubilized microsomes, followed by sucrose gradient centrifugation (Fig. S1 B). RyR2 identity in our single-channel experiments was confirmed pharmacologically (Fig. S8). The cytosolic Ca^{2+} sensitivity of single WT and K4750Q RyR2s is compared in Fig. 7. Low luminal-side Ca^{2+} (pCa = 7) used here did not activate the channels (Fig. 9 B). The WT RyR2 activated between pCa_{cyt} 5 and 2 with its open probability (Po) peaking at pCa_{cyt} 4.5 and then falling to near zero at pCa_{cyt} 2. In contrast, K4750Q was active at a lower $[Ca^{2+}]_{cyt}$ (pCa_{cyt} 6) and remained continuously open (Po near unity) at pCa_{cyt} between 4.5 and 2. Single K4750Q RyR2 channels showed no evidence of $[Ca^{2+}]_{cyt}$ inactivation. The absence of Ca^{2+} inactivation

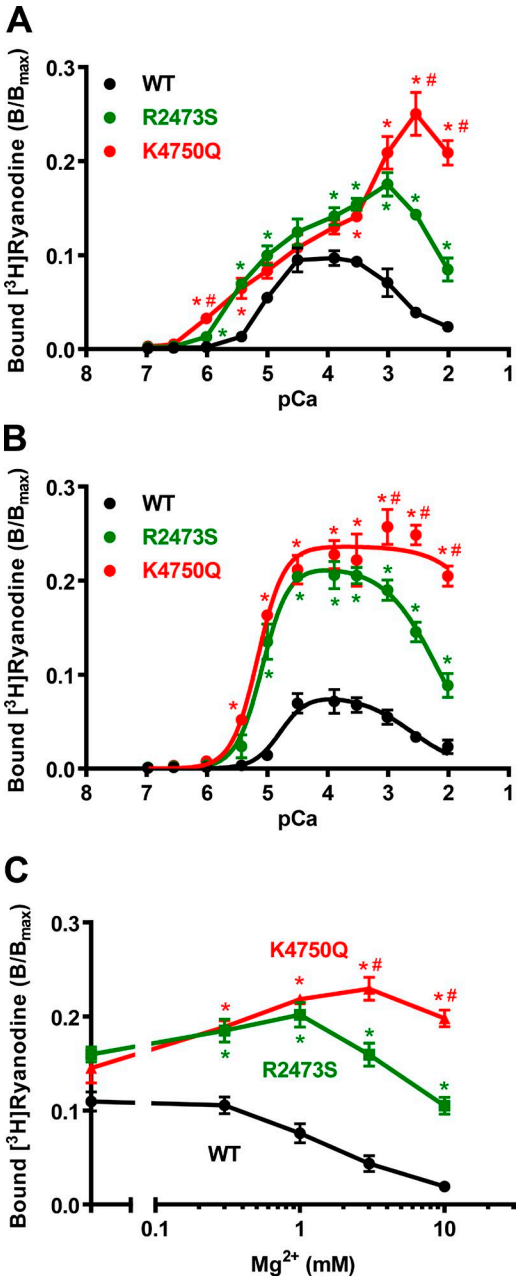

Figure 6. **Ca^{2+} and Mg^{2+} dependences of [^{3}H]ryanodine binding to microsomes from RyR2-expressing HEK293 cells.** (A and B) Dose-dependent action of Ca^{2+} on binding in the absence (A) and presence (B) of 1 mM Mg^{2+}. Binding data in WT (black), R2473S (green), and K4750Q (red) are shown in each graph. (C) Dose-dependent effect of Mg^{2+} on binding at pCa 4. Means of triplicate determinations were plotted. Statistical testing was done by one-way ANOVA. *, $P < 0.05$ (K4750Q vs. WT). #, $P < 0.05$ (K4750Q vs. R2473S). Values shown are mean ± SEM.

at high $[Ca^{2+}]_{cyt}$ resulted in prolonged openings. Fig. 7 B summarizes the relationships between RyR2 Po and $[Ca^{2+}]_{cyt}$ of recombinant WT and K4750Q RyR2s as well as native WT RyR2s isolated from cardiac muscle. The recombinant and native WT RyR2s had similar bell-shaped cytosolic Ca^{2+} sensitivities. The cytosolic Ca^{2+} EC_{50} of K4750Q was shifted more than one order of magnitude to 2.72 ± 0.09 µM (n_1 = 3.0 ± 0.0) compared with that of the WT RyR2 (32.4 ± 2.3 µM; n_1 = 1.8 ± 0.2). The cytosolic Ca^{2+} IC_{50} of WT was 468 ± 41 µM (n_2 = 1.3 ± 0.2). There was no cytosolic Ca^{2+} IC_{50} for K4750Q. To our knowledge, this is the first report of a point mutation that abolishes RyR2 cytosolic Ca^{2+} inactivation. Compared with K4750Q, the R2473S mutation resulted in much subtler alterations of cytosolic Ca^{2+} activation and inactivation.

The dwell time distributions of WT and K4750Q RyR2s (when activated by pCa_{cyt} 5) were best described by the sum of three closed and two open exponential components (Fig. 8 A). K4750Q mutation shifted both the peaks of closed and open time histograms to the left and right, respectively. The top-ranked kinetic schemes for WT and K4750Q (Fig. 8 B) were like that proposed by Mukherjee et al. (2012). One of the closed states (i.e., C_3) could be assigned to a "flickering" closed state (C_F) that arises from a Ca^{2+}-bound open state. Time constants and relative areas of all components are summarized in Table S2. This analysis suggests that K4750Q has markedly faster closed-to-open transitions but also slower open-to-closed transitions compared with WT, resulting in the prolonged openings observed (Fig. 7 A). The rate of the forward transition from O_2 to C_F markedly decreased, whereas that of the C_F to O_2 backward transition was not much changed by mutation. Finally, model-based simulated WT and K4750Q current traces (Fig. 8 C) resemble our experimental results, validating this analysis (Fig. 7 A).

We also examined the kinetics of Ca^{2+}-dependent inactivation in WT and K4750Q RyR2 channels (Figs. S9 and S10). The number of open states increased from two to three when $[Ca^{2+}]_{cyt}$ was increased from pCa 5 to pCa 4 or 3 (Fig. S10, A and B). In WT, inactivation was clear at pCa_{cyt} 3, and transition rates to closed states (i.e., O_2 to C_F & O_1 to C_2) became considerably faster, shortening the open dwell time (Fig. S10 B) to explain the Ca^{2+}-dependent inactivation. In K4750Q, elevating pCa_{cyt} to 4.8 resulted in extremely long-lived open states (experimental traces not depicted), and this was associated with marked slowing of the transition rates to the closed states (Fig. S10 C). It was impossible to generate K4750Q open/closed dwell time histograms to assess at higher $[Ca^{2+}]$ because they were almost always open (Fig. S10 D). But, those very long openings could be simulated assuming that the transition rates to the closed stated (O_2 to C_F and O_1 to C_2) were decreased threefold (Fig. 7 A).

The luminal Ca^{2+} action on single WT and K4750Q RyR2s is shown in Fig. 9 A. The pCa_{cyt} was 7, so there was no substantial cytosolic Ca^{2+} activation. Elevating luminal Ca^{2+} from 1 µM to 1 mM (pCa_{lum} 6 to 3) had no appreciable effect on WT RyR2 activity. In contrast, the same pCa_{lum} change dramatically activated the K4750Q RyR2. The K4750Q RyR2 activated by luminal Ca^{2+} characteristically had much longer closures compared with K4750Q RyR2 activated by cytosolic Ca^{2+} (Fig. 7 A). To discriminate the contribution of Ca^{2+} flux feed-through from a true luminal Ca^{2+} action, this was performed at two potentials (±20 mV) to change the lumen-to-cytosolic Ca^{2+} flux through the open RyR2. Luminal pCa 5 substantially prolonged K4750Q open time at 20 mV (flux in lumen-to-cytosol direction), but not −20-mV flux (flux in opposite direction). Note that the unitary RyR2 current amplitude is smaller at pCa_{lum} 3 because Ca^{2+} competes with the primary charge carrier (K^+) for occupancy of the pore (Tu et al., 1994).

The pCa_{lum} dependence of Po of WT, R2473S, and K4750Q is summarized in Fig. 9 B. The WT RyR2 was largely insensitive to pCa_{lum} (EC_{50} = 97 ± 16 mM; n_1 = 2.7 ± 0.5 at 20 mV). This might be explained by the absence of calsequestrin in the HEK293 cells. The R2473S channel was a bit more sensitive than WT to pCa_{lum} (EC_{50} = 83 ± 22 mM; n_1 = 0.9 ± 0.1 at 20 mV). However, K4750Q was highly sensitive to pCa_{lum} changes with an EC_{50} (at 20 mV) in the micromolar range. This change in sensitivity to pCa_{lum} is caused by an alteration in the "true" luminal Ca^{2+} sensitivity because lumen-to-cytosolic Ca^{2+} flux was the same in each case (i.e., membrane potential was 20 mV in each case). The K4750Q mutation renders the RyR2 exceptionally responsive to elevated luminal Ca^{2+} levels. The K4750Q has heightened cytosolic Ca^{2+} sensitivity (see Fig. 7 B), so the K4750Q channel might also be unusually sensitive to Ca^{2+} feed-through activation, where Ca^{2+} passes through the open channel and acts upon the cytosolic Ca^{2+} activation site of the channel (see review by Bers [2014]). To test this possibility, we measured the pCa_{lum} dependence of Po of K4750Q channels at −20 mV, a potential where Ca^{2+} feed-through activation will be minimal. The luminal Ca^{2+} EC_{50} of the K4750Q at −20 mV was 4.5 ± 0.1 mM (n_1 = 0.8 ± 0.0). This is still 18-fold greater than that of the R2473S channel at 20 mV (a potential where substantial Ca^{2+} feed-through may occur). To illustrate the feed-through contribution, we replotted the 20 and −20-mV K4750Q results as a function of lumen-to-cytosolic Ca^{2+} flux amplitude instead of luminal Ca^{2+} concentration (Fig. 9 B, right). This flux was calculated from the combination of Poisson-Nerst-Planck/density functional theory (PNP/DFT) permeation model and SR equivalent circuit analysis as described previously (Gillespie and Fill, 2008). When plotted against Ca^{2+} flux amplitude, the membrane potential dependence of the luminal Ca^{2+} action on K4750Q essentially disappears, indicating that

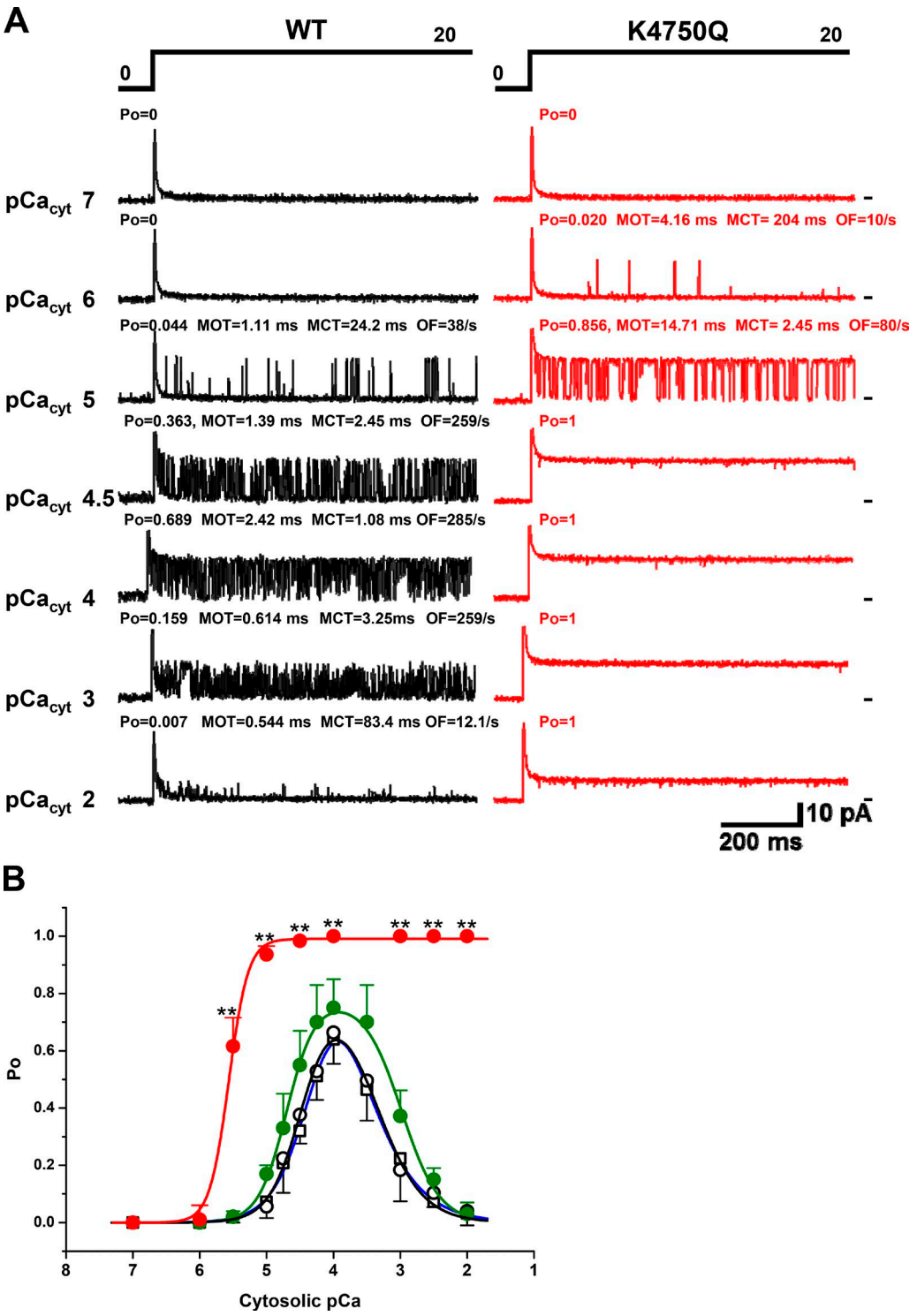

Figure 7. **Cytosolic Ca^{2+} action on single RyR2 function.** (A) Representative single-channel currents from WT (left) and K4750Q (right) channels. Openings are upward from the basal current level. (B) Summary of Po dependence on cytosolic Ca^{2+}. WT (black open circles), K4750Q (red filled circles), R2473S (green filled circles), and native RyR2 (black open squares). *n* = 9 (WT), 6 (K4750Q), 6 (R2473S), and 4 (native RyR2). **, P < 0.01 versus WT. Values shown are mean ± SEM.

K4750Q is indeed quite sensitive to Ca^{2+} feed-through activation. Thus, Ca^{2+} feed-through enhances the already altered "true" luminal Ca^{2+} sensitivity of the K4750Q channel.

We also examined the kinetics of luminal Ca^{2+} regulation of WT and K4750Q RyR2 channels. At pCa_{lum} 4, the dwell time distributions of WT and K4750Q RyR2s were best described by the sum of three closed and three

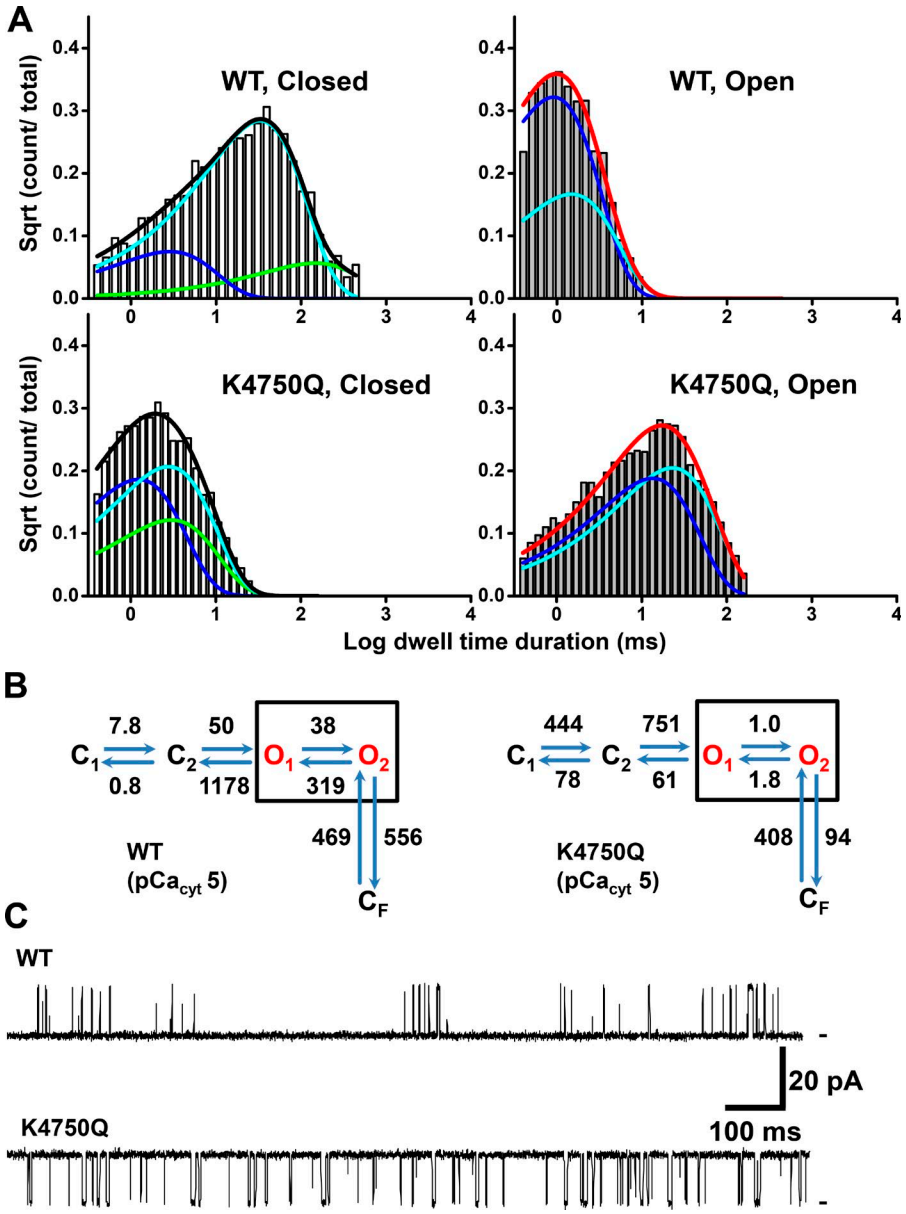

Figure 8. **K4750Q mutation-driven kinetic alterations in cytosolic Ca^{2+} activated channels.** (A) Dwell time distributions (pCa$_{cyt}$ 5) from WT and K4750Q. (B) State models of WT and K4750Q. (left) WT: maximum likelihood value (LL) = 16,270, events = 3,928; (right) K4750Q: LL = 7,343, events = 1,734. (C) Model-based simulated traces from WT and K4750Q. *n* = 6 for WT and mutant channels.

open exponential components (Fig. 10 A and Table S2). Luminal Ca^{2+} activation of RyR2-K4750Q shifted both closed and open time histograms to the right (compared with WT). In contrast, cytosolic Ca^{2+} activation shifted K4750Q closed histogram in the opposite left direction relative to the WT (Fig. 8 A). This was attributable to the shorter closings in the cytosolic Ca^{2+}-activated K4750Q (Figs. 7 A and 8 C). Both cytosolic and luminal Ca^{2+} activation increased the K4750Q closed to open (C_1 to O_1) transition rates and decreased the K4750Q open to closed (O_2 to C_F and O_1 to C_2) transition rates (Fig. 10 B), yielding stabilized openings (Fig. 7 A, Fig. 8 C, Fig. 9 A [bottom], and Fig. 10 C). However, the transition rate from C_F to C_2 was also markedly slowed in luminal Ca^{2+}-activated K4750Q channels, yielding long-lived closings (Fig. 9 A [bottom] and Fig. 10 C). Thus, the K4750Q RyR2's transition rates between O_2 and C_F are altered unidirectionally when the channel is activated by cytosolic Ca^{2+} (Fig. 8 B) but bidirectionally when it is activated by luminal Ca^{2+} (Fig. 10 B). Simulated current traces of WT and K4750Q activated by luminal Ca^{2+} (Fig. 10 C) were identical to the experimental traces (Fig. 9 A).

DISCUSSION

The CPVT phenotype observed in RyR2-K4650Q mutation carrier is among the worst we know about. Polymorphic VT was easily induced by daily exercise (such as climbing a single flight of stairs). Measurements of cytosolic and intra-SR Ca^{2+} here revealed that the RyR2-K4750Q mutation profoundly alters Ca^{2+} handling in HEK293 cells. The mutation simultaneously results in a decrease in the SR Ca^{2+} load and an increase in sponta-

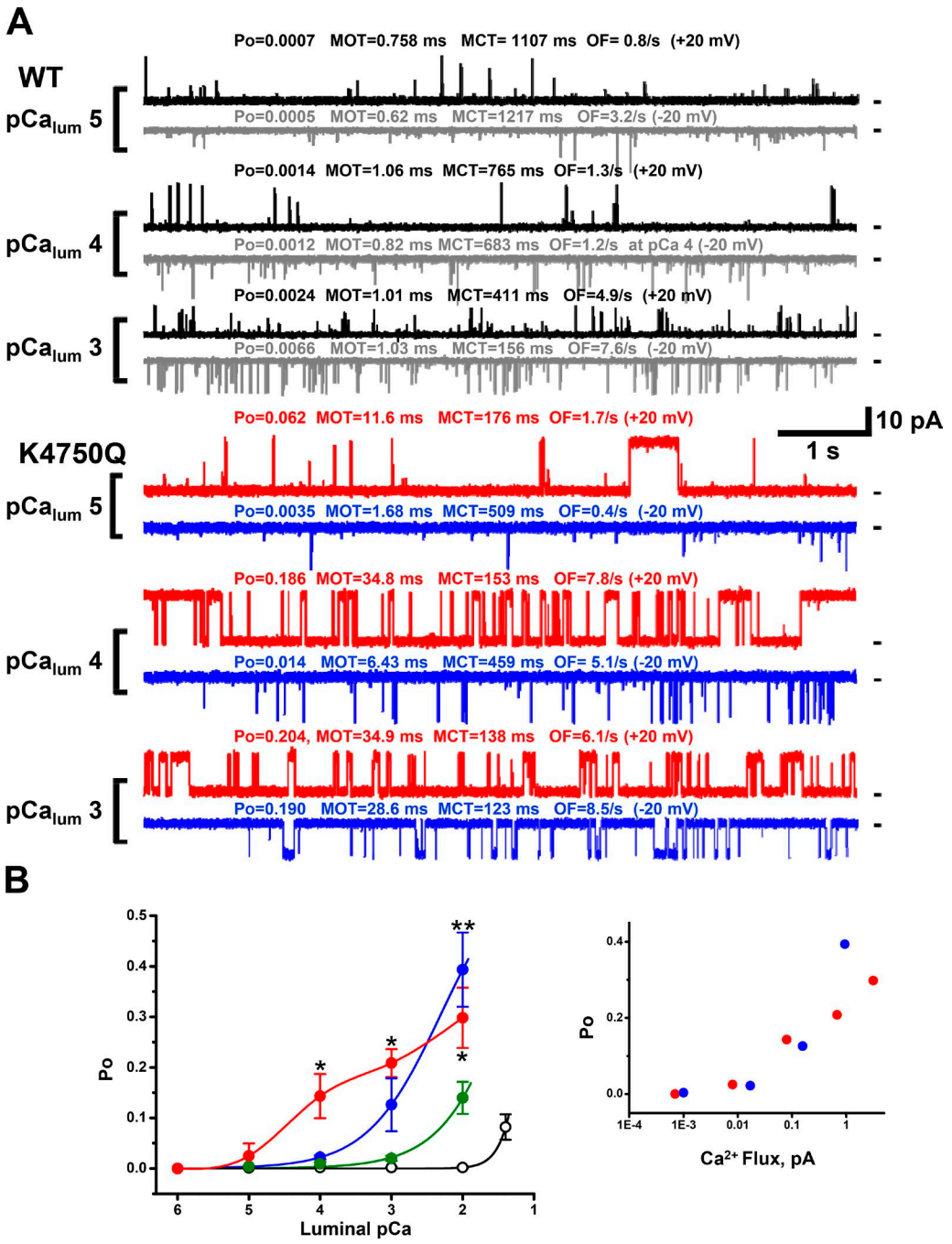

Figure 9. **Luminal Ca^{2+} action on single RyR2 function.** (A) Representative single-channel currents from WT (top) and K4750Q (bottom) recorded at 20 and −20 mV. (B) Summary of the luminal Ca^{2+} dependence of Po in WT (20 mV, black open circles), R2473S (20 mV, green filled circles), K4750Q (20 mV, red filled circles), and K4750Q (−20 mV, blue filled circles). *n* = 6 for WT and mutant channels. *, P < 0.05 versus WT. **, P < 0.01 versus WT. The right panel replots K4750Q Po as a function of unitary RyR2 Ca^{2+} flux amplitude (pA). Values shown are mean ± SEM.

neous Ca^{2+} oscillation frequency, compared with WT. The commonly studied RyR2-R2473S mutation alters these same parameters but to a significantly smaller extent (Jiang et al., 2005). In vitro, the RyR2 dysfunction caused by the K4750Q was also significantly greater than that caused by the R2473S mutation. The clinical CPVT phenotype and the intracellular Ca^{2+} handling dysfunction caused by the RyR2-K4750Q mutation are dramatic and likely approach the survivable limit, establishing the extent of the clinical CPVT spectrum.

The intracellular Ca^{2+} handling dysfunction caused by the RyR2-K4750Q mutation was defined here using a recently developed ER-targeted Ca^{2+}-sensing protein, R-CEPIA1 (Suzuki et al., 2014). The more commonly

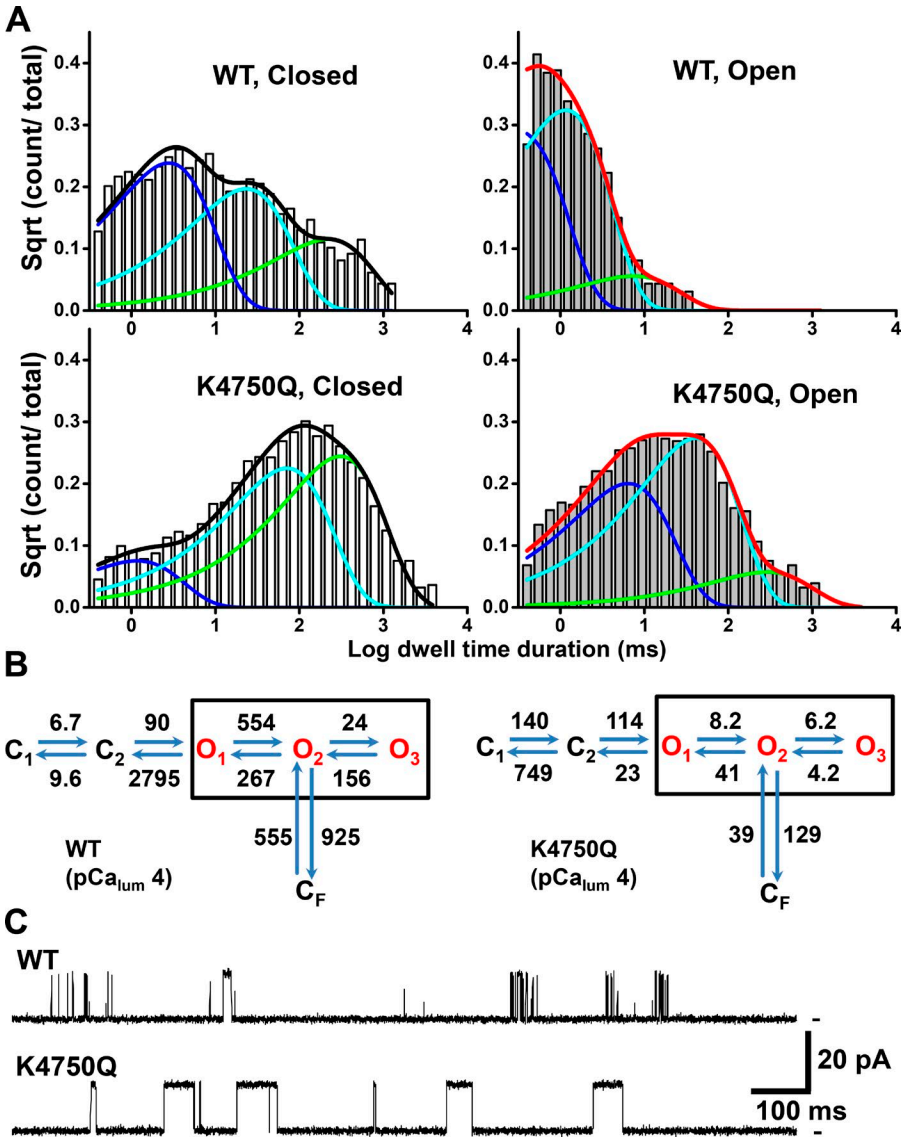

Figure 10. **K4750Q mutation-driven kinetic alterations in luminal Ca^{2+} activated channels.** (A) Dwell time distributions (pCa_{lum} 4) from WT and K4750Q. (B) State models of WT and K4750Q. (left) WT: maximum likelihood value (LL) = 9,802, events = 2,133; (right) K4750Q: LL = 7,083, events = 3,886. (C) Model-based simulated traces from WT and K4750Q. *n* = 6 for WT and mutant channels.

used indicator is D1ER, a ratiometric FRET-based ER-targeted luminal Ca^{2+} sensor (K_d ~60 µM). R-CEP IA1er has substantially lower Ca^{2+} affinity (K_d = 455 µM in situ) and is a single wavelength excitation/single wavelength emission type indicator. Co-expressing R-CEPIA1er and G-GECO1.1 here permitted simultaneously measurements of $[Ca^{2+}]_{lum}$ and $[Ca^{2+}]_{cyt}$ signals via RyR2s for the first time using dual genetically encoded indicators. This dual genetically encoded indicator approach could be exploited in future genetically altered disease models.

Effects of the K4750Q mutation on Ca^{2+} homeostasis

Our results demonstrate the dramatic action of the K4750Q mutation on Ca^{2+} homeostasis in HEK293 cells (Figs. 3 and 5 and Figs. S3, S4, and S5). Frequency of Ca^{2+} oscillations was three times higher, and $[Ca^{2+}]_{lum}$ was decreased to 1/3 (compared with WT) 24 h after induction. The increase in oscillation frequency was observed even 2 h after K4750Q, but not WT, induction. At this 2-h time point, RyR2 expression was relatively low and $[Ca^{2+}]_{lum}$ was not substantially lowered. This suggests that $[Ca^{2+}]_{lum}$ is affected by both RyR2 expression level and the RyR2's functional attributes. It is unclear whether $[Ca^{2+}]_{lum}$ is reduced in cardiomyocytes of the patient carrying the heterozygous K4750Q mutation. The fact that $[Ca^{2+}]_{lum}$ of cardiomyocytes from heterozygous R2473S mice do have slightly but significantly reduced $[Ca^{2+}]_{lum}$ (Uchinoumi et al., 2010) suggests that heterozygous expression of K4750Q may also reduce $[Ca^{2+}]_{lum}$. However, the K4750Q patient had no indication of heart failure or abnormal morphology, and this suggests that the change in $[Ca^{2+}]_{lum}$ is modest, if any. Because the K4750Q patient is heterozygous, both WT and mutant RyR2 proteins are present in heart. How (or if) these proteins form homo- and/or heterotetramers is not clear. To our knowledge, this is also the case for other analogous human CPVT heterozygous RyR2

mutations as well. Heterotetrameric RyR2s would likely exhibit a milder phenotype. The SR containing a mixture of WT and mutant homotetrameric RyR2 would also likely exhibit a milder disease phenotype. Indeed, we observed a milder phenotype in HL-1 cells that contain both WT and mutant RyR2 protein (as compared with that in HEK293 cells that only contain homotetrameric mutant channels). In contrast, the susceptibility of spontaneous Ca^{2+} wave was consistently observed at any $[Ca^{2+}]_{lum}$ in both HEK293 cells (Fig. S5) and in HL-1 cells (Fig. 4 F). Furthermore, the frequency of the spontaneous Ca^{2+} oscillation was increased under Ca^{2+} overload conditions.

Our K4750Q mutation results suggest that the $[Ca^{2+}]_{lum}$ threshold for Ca^{2+} release is not the sole factor that determines K4750Q spontaneous Ca^{2+} release frequency because the frequency was high at all ER Ca^{2+} levels (Fig. S5). Instead, spontaneous Ca^{2+} release frequency is likely determined by a balance of four parameters; rates of Ca^{2+} influx, efflux, Ca^{2+} uptake to SR/ER, and Ca^{2+} release via RyR2. Thus, multiple functional defects caused by the K4750Q mutation likely explain the severe arrhythmia propensities in ventricle and atrium of the K4750Q patient.

The K4750Q mutation causes multiple RyR2 functional defects

We show that the K4750Q mutation simultaneously caused the RyR2 to activate at lower cytosolic Ca^{2+} levels, abolished RyR2 cytosolic Ca^{2+}/Mg^{2+} inactivation, and made RyR2 hypersensitive to luminal Ca^{2+} activation. Any one of these defects alone could theoretically promote RyR2-mediated SR Ca^{2+} leak and diastolic Ca^{2+}-evoked arrhythmias. The synergy of these defects explains the exceptionally severe CPVT and intracellular Ca^{2+} handling dysfunction observed.

Multiple functional defects induced by a single point mutation (K4750Q) imply that this residue influences a pivotal region of the RyR2 protein, a locus where multiple regulatory inputs converge to control the RyR2 gate. In other words, the K4750 point mutation disrupts how signals (arising from three different regulatory sites) get conveyed to the RyR2 gate. This idea is consistent with the known near-atomic resolution RyR structure (Yan et al., 2015). The K4750 residue (corresponding to K4821 in RyR1) is located just before the S4–5 linker (Fig. 2). Specifically, it is located in a turn between two α-helices of the RyR2's S4 segment and S4–5 linker (Yan et al., 2015). Consequently, the four K4750 residues in the channel tetramer surround the central pore that is formed by the S5 and 6 segments. Elegant works with central core disease– and malignant hyperthermia–causing RyR1 mutations (Sambuughin et al., 2005; Yan et al., 2015) and CPVT-causing RyR2 mutation (Yan et al., 2015) indicate that the S4 segment and S4–5 linker play an important role in RyR gating (Murayama et al., 2011; Ramachandran et al., 2013). The K4750Q mutation proximity to the gate may in part explain exceptionally severe phenotype (compared with the R2473S mutation). However, we do not believe there is a clear relationship between RyR2 mutation-to-pore distance and functional phenotype.

The transmembrane helices of RyR that form its pore resemble those that form the pore of the bacterial Na^{+} channel (Efremov et al., 2015). In the bacterial channel, Yarov-Yarovoy et al. (2012) proposed that conformational changes of the intracellular half of the S4 segment during activation are rigidly coupled to the lateral movement of the S4–5 linker, inducing S5 and S6 movement and subsequently channel opening. Thus, the K4750 residue may have an analogous action on the RyR2 S4 segment and S4–5 linker. Indeed, the basic K4750 residue in the S4 segment could form a salt bridge with some acidic residue in the S5 segment of the same or adjacent protomer, stabilizing the closed state. Exchange for a neutral residue (i.e., K4750Q) could destabilize the closed state of RyR2, explaining the substantial diastolic Ca^{2+} leak associated with K4750Q CPVT. This explanation of our functional results is consistent with that of Yan et al. (2015). The RyR structural prediction that the S4–5 linker interacts with the pore likely allosterically regulates its opening.

An alternative explanation for how the K4750Q mutation simultaneously alters cytosolic Ca^{2+} activation, cytosolic Ca^{2+}/Mg^{2+} inactivation and luminal Ca^{2+} activation is that the K4750Q point mutation somehow alters the affinity/efficacy of all three sites. This is theoretically possible but unlikely. Because we did not measure the Ca^{2+}/Mg^{2+} affinity of these sites, we cannot definitively rule out this alternative possibility.

Mg^{2+} action on K4750Q RyR2 channels

Mg^{2+} acts as a competitive inhibitor at the RyR2 cytosolic Ca^{2+} activation site. Ca^{2+} and Mg^{2+} have nearly equal affinity and efficacy at the cytosolic RyR2 inactivation site. Together, this explains the inhibitory influence on WT RyR2 function. Interestingly, Mg^{2+} significantly increased [^{3}H]ryanodine binding to RyR2-K4750Q and -R2473S (Fig. 6 and Fig. S7), indicative of Mg^{2+} activation. A similar Mg^{2+} activation phenomenon was reported (Chugun et al., 2007) in rat and rabbit WT SR microsomes as well, and the authors proposed that the Mg^{2+} activation was caused by a third class of cytosolic divalent cation binding site, the "third effect." Recently, Gomez and Yamaguchi (2014) proposed that Mg^{2+} acting at the RyR2's cytosolic EF-hand domains might explain the third effect. We did not observe this third effect for the WT RyR2 but was clear for the RyR2-K4750Q and -R2473S channels, implying that these mutations may either unmask or promote the phenomenon. However, further investigations are needed to clarify the underlying mechanisms involved in the third effect.

Relief from Mg^{2+} inhibition is a frequent consequence of RyR2 and RyR1 missense mutations (e.g., P2328S, Q4201R, and V4653F for RyR2 [Lehnart et al., 2004] and R615C for RyR1 [Laver et al., 1997b]). These RyR2 mutations change the cytosolic Mg^{2+} IC_{50} ∼1.9-fold. Here, K4750Q changed the cytosolic Mg^{2+} IC_{50} ∼6.6-fold (i.e., 1.5 in WT to 10 mM in the mutant). This large loss of Mg^{2+} inhibition could arise from reduced cytosolic inactivation site Mg^{2+} affinity/efficacy or uncoupling of its action from the pore. Unlike the other mutants that partially relieve Mg^{2+} inhibition, the K4750Q mutation in effect abolished cytosolic Ca^{2+}/Mg^{2+} inactivation. Because K4750Q also altered RyR2's cytosolic Ca^{2+} activation and luminal Ca^{2+} regulation, functional uncoupling of the inactivation site from the gate appears to be the most likely explanation for our results.

Gating models of single RyR2 channels

Several kinetic models based on RyR2 single-channel current measurements were proposed previously (Sachs et al., 1995; Stern et al., 1999; Mukherjee et al., 2012). Only the Mukherjee et al. (2012) model estimated rate constants from open and closed time distributions, chose state models on the basis of statistical evaluation, and ranked prospective models. However, this group modeled just cytosolic RyR2-WT Ca^{2+} activation. Applying the approach of Mukherjee et al. (2012) approach, we constructed kinetic schemes for both RyR2-WT and -K4750Q cytosolic Ca^{2+} activation/inactivation as well as luminal Ca^{2+} regulation (Figs. 8 and 10). This modeling successfully reproduced the single-channel kinetics of the RyR2-WT and -K4750Q channels. The modeling revealed that the K4750Q mutation strongly stabilizes the open state of cytosolic and luminal Ca^{2+} activated channel as well as essentially locked the RyR2 in the open configuration at high cytosolic Ca^{2+} levels (i.e., abolished Ca^{2+}-dependent inactivation; Fig. S10). This stabilization of the open state and the resulting Po increase explain the substantial leftward shift in cytosolic/luminal RyR2-K4750Q Ca^{2+} sensitivity (Figs. 7 B and 9 B). Modeling using previously reported circular and linear kinetic RyR2 schemes (Sachs et al., 1995; Stern et al., 1999) did not converge and thus failed to explain our results. Thus, the RyR2 kinetic schemes presented here more accurately reflect RyR2 Ca^{2+} control and consequently will be important to understanding the operation of the RyR2 store sensing gate (Chen et al., 2014; SR luminal Ca^{2+} binding site) that governs Ca^{2+} waves and Ca^{2+}-triggered arrhythmias.

Uniqueness of K4750Q RyR2 dysfunction

The multifaceted dysfunction caused by the K4750Q mutation is unique, compared with previously studied RyR2 CPVT mutations. Generally, there are two categories of CPVT causing RyR2 dysfunction. Most CPVT mutations alter RyR2 luminal Ca^{2+} activation but leave its cytosolic Ca^{2+} sensitivity unchanged. This category includes RyR2-R4496C (Jiang et al., 2002), -N4895D (Jiang et al., 2004), -S2246L, -R2474S, -Q4201R, and -I4867M (Jiang et al., 2005). A few RyR2 mutations alter both RyR2 luminal Ca^{2+} activation and the cytosolic Ca^{2+} EC_{50}. This category includes RyR2-G230C (Liu et al., 2013), -V2475F (Loaiza et al., 2013), and -N4104K (Jiang et al., 2004). To the best of our knowledge, the K4750Q mutation is the first CPVT mutation identified that alters (abolishes) RyR2 cytosolic Ca^{2+} inactivation, to the best of our knowledge. K4750Q is thus the first member of a new category of CPVT-causing mutations of RyR2 (category three). Furthermore, the degree to which K4750Q shifts RyR2 cytosolic Ca^{2+} EC_{50} is also quite unique. The G230C (Liu et al., 2013), V2475F (Loaiza et al., 2013), and N4104K (Jiang et al., 2004) CPVT mutations shift cytosolic Ca^{2+} EC_{50} two- to threefold. The K4750Q mutation shifts cytosolic Ca^{2+} EC_{50} 16-fold (compared with WT). This is the greatest magnitude RyR2 dysfunction known to be caused by a CPVT RyR2 mutation to date. Lastly, Tang et al. (2012) proposed that abnormal RyR2 Ca^{2+} release termination is a common defect of RyR2 mutations associated with cardiomyopathies but not those associated with CPVT. They showed that fractional release (i.e., difference between spontaneous SR Ca^{2+} release activation and termination threshold) was increased by cardiomyopathy-linked RyR2 mutations but was unaltered by CPVT-linked RyR2 mutations (E189D and R4496C). Here, we found that the K4750Q mutation uniquely decreased both spontaneous SR Ca^{2+} release activation and termination threshold as well as fractional release (unlike the CPVT mutations tested by Tang et al. [2012]).

Conclusion

We conducted the first functional analyses of novel CPVT-causing mutation, RyR2-K4750Q. This RyR2 point mutation simultaneously modifies multiple RyR2-resident control mechanisms (cytosolic Ca^{2+} activation, cytosolic Ca^{2+}/Mg^{2+} inactivation, and luminal Ca^{2+} regulation, implying that the K4750 residue resides at a locus in the RyR2 structure influences the transduction of multiple regulatory inputs to RyR2 gate operation. The degree of RyR2 dysfunction caused by the K4750Q mutation is larger than that caused by other known CPVT RyR2 mutation. This explains the exceptionally severe CPVT clinical phenotype observed. This severity of the CPVT phenotype and extent of intracellular Ca^{2+} handling dysfunction caused by the RyR2-K4750Q mutation are likely near the survivable limit. Consequently, our findings will likely be key as new RyR2-targeted anti-CPVT therapeutic strategies are developed.

ACKNOWLEDGMENTS

We thank Drs. Junji Suzuki (Tokyo University), Akira Honda (Fukuoka University), and Junichi Nakai (Saitama University) for valuable discussions.

This study was supported by a Ministry of Education, Culture, Sports, Science and Technology, Japan Grant-in-Aid for Scientific Research (26460305 to A. Uehara, 24590330 and 16K08507 to T. Murayama, and 15K08243 to N. Kurebayashi) and by another one on Innovative Areas, HD Physiology (23136514 and 25136718 to N. Kurebayashi). It was also subsidized by other funds from the Central Research Institute of Fukuoka University (to A. Uehara), the Vehicle Racing Commemorative Foundation (to N. Kurebayashi), and the Institute of Seizon & Life Sciences (to T. Murayama). M. Fill was supported by National Institutes of Health grants (HL057832, AR054098, and GM111397).

The authors declare no competing financial interests.

Eduardo Ríos served as editor.

Submitted: 18 May 2016
Revised: 19 October 2016
Accepted: 7 December 2016

REFERENCES

Bers, D.M. 2014. Cardiac sarcoplasmic reticulum calcium leak: basis and roles in cardiac dysfunction. *Annu. Rev. Physiol.* 76:107–127. http://dx.doi.org/10.1146/annurev-physiol-020911-153308

Cerrone, M., B. Colombi, M. Santoro, M.R. di Barletta, M. Scelsi, L. Villani, C. Napolitano, and S.G. Priori. 2005. Bidirectional ventricular tachycardia and fibrillation elicited in a knock-in mouse model carrier of a mutation in the cardiac ryanodine receptor. *Circ. Res.* 96:e77–e82. http://dx.doi.org/10.1161/01.RES.0000169067.51055.72

Chen, W., R. Wang, B. Chen, X. Zhong, H. Kong, Y. Bai, Q. Zhou, C. Xie, J. Zhang, A. Guo, et al. 2014. The ryanodine receptor store-sensing gate controls Ca^{2+} waves and Ca^{2+}-triggered arrhythmias. *Nat. Med.* 20:184–192. http://dx.doi.org/10.1038/nm.3440

Cheng, H., W.J. Lederer, and M.B. Cannell. 1993. Calcium sparks: elementary events underlying excitation-contraction coupling in heart muscle. *Science.* 262:740–744. http://dx.doi.org/10.1126/science.8235594

Chu, A., M. Díaz-Muñoz, M.J. Hawkes, K. Brush, and S.L. Hamilton. 1990. Ryanodine as a probe for the functional state of the skeletal muscle sarcoplasmic reticulum calcium release channel. *Mol. Pharmacol.* 37:735–741.

Chugun, A., K. Taniguchi, T. Murayama, T. Uchide, Y. Hara, K. Temma, Y. Ogawa, and T. Akera. 2003. Subcellular distribution of ryanodine receptors in the cardiac muscle of carp (*Cyprinus carpio*). *Am. J. Physiol. Regul. Integr. Comp. Physiol.* 285:R601–R609. http://dx.doi.org/10.1152/ajpregu.00419.2002

Chugun, A., O. Sato, H. Takeshima, and Y. Ogawa. 2007. Mg^{2+} activates the ryanodine receptor type 2 (RyR2) at intermediate Ca^{2+} concentrations. *Am. J. Physiol. Cell Physiol.* 292:C535–C544. http://dx.doi.org/10.1152/ajpcell.00275.2006

Claycomb, W.C., N.A. Lanson Jr., B.S. Stallworth, D.B. Egeland, J.B. Delcarpio, A. Bahinski, and N.J. Izzo Jr. 1998. HL-1 cells: a cardiac muscle cell line that contracts and retains phenotypic characteristics of the adult cardiomyocyte. *Proc. Natl. Acad. Sci. USA.* 95:2979–2984. http://dx.doi.org/10.1073/pnas.95.6.2979

Efremov, R.G., A. Leitner, R. Aebersold, and S. Raunser. 2015. Architecture and conformational switch mechanism of the ryanodine receptor. *Nature.* 517:39–43. http://dx.doi.org/10.1038/nature13916

Fabiato, A. 1983. Calcium-induced release of calcium from the cardiac sarcoplasmic reticulum. *Am. J. Physiol.* 245:C1–C14.

Gillespie, D., and M. Fill. 2008. Intracellular calcium release channels mediate their own countercurrent: the ryanodine receptor case study. *Biophys. J.* 95:3706–3714. http://dx.doi.org/10.1529/biophysj.108.131987

Gomez, A.C., and N. Yamaguchi. 2014. Two regions of the ryanodine receptor calcium channel are involved in Ca^{2+}-dependent inactivation. *Biochemistry.* 53:1373–1379. http://dx.doi.org/10.1021/bi401586h

Guo, T., D. Gillespie, and M. Fill. 2012. Ryanodine receptor current amplitude controls Ca^{2+} sparks in cardiac muscle. *Circ. Res.* 111:28–36. http://dx.doi.org/10.1161/CIRCRESAHA.112.265652

Jiang, D., B. Xiao, L. Zhang, and S.R. Chen. 2002. Enhanced basal activity of a cardiac Ca^{2+} release channel (ryanodine receptor) mutant associated with ventricular tachycardia and sudden death. *Circ. Res.* 91:218–225. http://dx.doi.org/10.1161/01.RES.0000028455.36940.5E

Jiang, D., B. Xiao, D. Yang, R. Wang, P. Choi, L. Zhang, H. Cheng, and S.R.W. Chen. 2004. RyR2 mutations linked to ventricular tachycardia and sudden death reduce the threshold for store-overload-induced Ca^{2+} release (SOICR). *Proc. Natl. Acad. Sci. USA.* 101:13062–13067. http://dx.doi.org/10.1073/pnas.0402388101

Jiang, D., R. Wang, B. Xiao, H. Kong, D.J. Hunt, P. Choi, L. Zhang, and S.R.W. Chen. 2005. Enhanced store overload-induced Ca^{2+} release and channel sensitivity to luminal Ca^{2+} activation are common defects of RyR2 mutations linked to ventricular tachycardia and sudden death. *Circ. Res.* 97:1173–1181. http://dx.doi.org/10.1161/01.RES.0000192146.85173.4b

Kawamura, M., S. Ohno, N. Naiki, I. Nagaoka, K. Dochi, Q. Wang, K. Hasegawa, H. Kimura, A. Miyamoto, Y. Mizusawa, et al. 2013. Genetic background of catecholaminergic polymorphic ventricular tachycardia in Japan. *Circ. J.* 77:1705–1713. http://dx.doi.org/10.1253/circj.CJ-12-1460

Laver, D.R., T.M. Baynes, and A.F. Dulhunty. 1997a. Magnesium inhibition of ryanodine-receptor calcium channels: evidence for two independent mechanisms. *J. Membr. Biol.* 156:213–229. http://dx.doi.org/10.1007/s002329900202

Laver, D.R., V.J. Owen, P.R. Junankar, N.L. Taske, A.F. Dulhunty, and G.D. Lamb. 1997b. Reduced inhibitory effect of Mg^{2+} on ryanodine receptor-Ca^{2+} release channels in malignant hyperthermia. *Biophys. J.* 73:1913–1924. http://dx.doi.org/10.1016/S0006-3495(97)78222-5

Lehnart, S.E., X.H. Wehrens, P.J. Laitinen, S.R. Reiken, S.X. Deng, Z. Cheng, D.W. Landry, K. Kontula, H. Swan, and A.R. Marks. 2004. Sudden death in familial polymorphic ventricular tachycardia associated with calcium release channel (ryanodine receptor) leak. *Circulation.* 109:3208–3214. http://dx.doi.org/10.1161/01.CIR.0000132472.98675.EC

Lindsay, A.R., S.D. Manning, and A.J. Williams. 1991. Monovalent cation conductance in the ryanodine receptor-channel of sheep cardiac muscle sarcoplasmic reticulum. *J. Physiol.* 439:463–480. http://dx.doi.org/10.1113/jphysiol.1991.sp018676

Liu, Y., L. Kimlicka, F. Hiess, X. Tian, R. Wang, L. Zhang, P.P. Jones, F. Van Petegem, and S.R. Chen. 2013. The CPVT-associated RyR2 mutation G230C enhances store overload-induced Ca^{2+} release and destabilizes the N-terminal domains. *Biochem. J.* 454:123–131. http://dx.doi.org/10.1042/BJ20130594

Loaiza, R., N.A. Benkusky, P.P. Powers, T. Hacker, S. Noujaim, M.J. Ackerman, J. Jalife, and H.H. Valdivia. 2013. Heterogeneity of ryanodine receptor dysfunction in a mouse model of catecholaminergic polymorphic ventricular tachycardia. *Circ. Res.* 112:298–308. http://dx.doi.org/10.1161/CIRCRESAHA.112.274803

Mukherjee, S., N.L. Thomas, and A.J. Williams. 2012. A mechanistic description of gating of the human cardiac ryanodine receptor

in a regulated minimal environment. *J. Gen. Physiol.* 140:139–158. http://dx.doi.org/10.1085/jgp.201110706

Murayama, T., and N. Kurebayashi. 2011. Two ryanodine receptor isoforms in nonmammalian vertebrate skeletal muscle: possible roles in excitation-contraction coupling and other processes. *Prog. Biophys. Mol. Biol.* 105:134–144. http://dx.doi.org/10.1016/j.pbiomolbio.2010.10.003

Murayama, T., N. Kurebayashi, and Y. Ogawa. 2000. Role of Mg^{2+} in Ca^{2+}-induced Ca^{2+} release through ryanodine receptors of frog skeletal muscle: modulations by adenine nucleotides and caffeine. *Biophys. J.* 78:1810–1824. http://dx.doi.org/10.1016/S0006-3495(00)76731-2

Murayama, T., N. Kurebayashi, T. Oba, H. Oyamada, K. Oguchi, T. Sakurai, and Y. Ogawa. 2011. Role of amino-terminal half of the S4-S5 linker in type 1 ryanodine receptor (RyR1) channel gating. *J. Biol. Chem.* 286:35571–35577. http://dx.doi.org/10.1074/jbc.M111.255240

Murayama, T., N. Kurebayashi, T. Yamazawa, H. Oyamada, J. Suzuki, K. Kanemaru, K. Oguchi, M. Iino, and T. Sakurai. 2015. Divergent activity profiles of type 1 ryanodine receptor channels carrying malignant hyperthermia and central core disease mutations in the amino-terminal region. *PLoS One.* 10:e0130606. http://dx.doi.org/10.1371/journal.pone.0130606

Murayama, T., N. Kurebayashi, H. Ogawa, T. Yamazawa, H. Oyamada, J. Suzuki, K. Kanemaru, K. Oguchi, M. Iino, and T. Sakurai. 2016. Genotype-phenotype correlations of malignant hyperthermia and central core disease mutations in the central region of the RYR1 channel. *Hum. Mutat.* 37:1231–1241. http://dx.doi.org/10.1002/humu.23072

Nicolai, C., and F. Sachs. 2013. Solving ion channel kinetics with the QuB software. *Biophys. Rev. Lett.* 08:191–211. http://dx.doi.org/10.1142/S1793048013300053

Priori, S.G., and S.R. Chen. 2011. Inherited dysfunction of sarcoplasmic reticulum Ca^{2+} handling and arrhythmogenesis. *Circ. Res.* 108:871–883. http://dx.doi.org/10.1161/CIRCRESAHA.110.226845

Priori, S.G., C. Napolitano, N. Tiso, M. Memmi, G. Vignati, R. Bloise, V. Sorrentino, and G.A. Danieli. 2001. Mutations in the cardiac ryanodine receptor gene (*hRyR2*) underlie catecholaminergic polymorphic ventricular tachycardia. *Circulation.* 103:196–200. http://dx.doi.org/10.1161/01.CIR.103.2.196

Qin, F., A. Auerbach, and F. Sachs. 1996. Estimating single-channel kinetic parameters from idealized patch-clamp data containing missed events. *Biophys. J.* 70:264–280. http://dx.doi.org/10.1016/S0006-3495(96)79568-1

Ramachandran, S., A. Chakraborty, L. Xu, Y. Mei, M. Samsó, N.V. Dokholyan, and G. Meissner. 2013. Structural determinants of skeletal muscle ryanodine receptor gating. *J. Biol. Chem.* 288:6154–6165. http://dx.doi.org/10.1074/jbc.M112.433789

Sachs, F., F. Qin, and P. Palade. 1995. Models of Ca^{2+} release channel adaptation. *Science.* 267:2010–2011. http://dx.doi.org/10.1126/science.7701327

Sambuughin, N., H. Holley, S. Muldoon, B.W. Brandom, A.M. de Bantel, J.R. Tobin, T.E. Nelson, and L.G. Goldfarb. 2005. Screening of the entire ryanodine receptor type 1 coding region for sequence variants associated with malignant hyperthermia susceptibility in the North American population. *Anesthesiology.* 102:515–521. http://dx.doi.org/10.1097/00000542-200503000-00007

Shaner, N.C., R.E. Campbell, P.A. Steinbach, B.N. Giepmans, A.E. Palmer, and R.Y. Tsien. 2004. Improved monomeric red, orange and yellow fluorescent proteins derived from *Discosoma* sp. red fluorescent protein. *Nat. Biotechnol.* 22:1567–1572. http://dx.doi.org/10.1038/nbt1037

Stern, M.D. 1992. Theory of excitation-contraction coupling in cardiac muscle. *Biophys. J.* 63:497–517. http://dx.doi.org/10.1016/S0006-3495(92)81615-6

Stern, M.D., L.S. Song, H. Cheng, J.S. Sham, H.T. Yang, K.R. Boheler, and E. Ríos. 1999. Local control models of cardiac excitation-contraction coupling. A possible role for allosteric interactions between ryanodine receptors. *J. Gen. Physiol.* 113:469–489. http://dx.doi.org/10.1085/jgp.113.3.469

Sugiyasu, A., Y. Oginosawa, A. Nogami, and Y. Hata. 2009. A case with catecholaminergic polymorphic ventricular tachycardia unmasked after successful ablation of atrial tachycardias from pulmonary veins. *Pacing Clin. Electrophysiol.* 32:e21–e24. http://dx.doi.org/10.1111/j.1540-8159.2009.02519.x

Suzuki, J., K. Kanemaru, K. Ishii, M. Ohkura, Y. Okubo, and M. Iino. 2014. Imaging intraorganellar Ca^{2+} at subcellular resolution using CEPIA. *Nat. Commun.* 5:4153. http://dx.doi.org/10.1038/ncomms5153

Tang, Y., X. Tian, R. Wang, M. Fill, and S.R. Chen. 2012. Abnormal termination of Ca^{2+} release is a common defect of RyR2 mutations associated with cardiomyopathies. *Circ. Res.* 110:968–977. http://dx.doi.org/10.1161/CIRCRESAHA.111.256560

Tani, H., M. Nishijima, H. Ushijima, T. Miyamura, and Y. Matsuura. 2001. Characterization of cell-surface determinants important for baculovirus infection. *Virology.* 279:343–353. http://dx.doi.org/10.1006/viro.2000.0699

Thomas, N.L., C.H. George, A.J. Williams, and F.A. Lai. 2007. Ryanodine receptor mutations in arrhythmias: advances in understanding the mechanisms of channel dysfunction. *Biochem. Soc. Trans.* 35:946–951. http://dx.doi.org/10.1042/BST0350946

Tu, Q., P. Velez, M. Cortes-Gutierrez, and M. Fill. 1994. Surface charge potentiates conduction through the cardiac ryanodine receptor channel. *J. Gen. Physiol.* 103:853–867. http://dx.doi.org/10.1085/jgp.103.5.853

Uchinoumi, H., M. Yano, T. Suetomi, M. Ono, X. Xu, H. Tateishi, T. Oda, S. Okuda, M. Doi, S. Kobayashi, et al. 2010. Catecholaminergic polymorphic ventricular tachycardia is caused by mutation-linked defective conformational regulation of the ryanodine receptor. *Circ. Res.* 106:1413–1424. http://dx.doi.org/10.1161/CIRCRESAHA.109.209312

Uehara, A., M. Fill, P. Vélez, M. Yasukochi, and I. Imanaga. 1996. Rectification of rabbit cardiac ryanodine receptor current by endogenous polyamines. *Biophys. J.* 71:769–777. http://dx.doi.org/10.1016/S0006-3495(96)79276-7

Welch, W., S. Rheault, D.J. West, and A.J. Williams. 2004. A model of the putative pore region of the cardiac ryanodine receptor channel. *Biophys. J.* 87:2335–2351. http://dx.doi.org/10.1529/biophysj.104.044180

Yamamoto, T., R. El-Hayek, and N. Ikemoto. 2000. Postulated role of interdomain interaction within the ryanodine receptor in Ca^{2+} channel regulation. *J. Biol. Chem.* 275:11618–11625. http://dx.doi.org/10.1074/jbc.275.16.11618

Yan, Z., X.C. Bai, C. Yan, J. Wu, Z. Li, T. Xie, W. Peng, C.C. Yin, X. Li, S.H.W. Scheres, et al. 2015. Structure of the rabbit ryanodine receptor RyR1 at near-atomic resolution. *Nature.* 517:50–55. http://dx.doi.org/10.1038/nature14063

Yarov-Yarovoy, V., P.G. DeCaen, R.E. Westenbroek, C.Y. Pan, T. Scheuer, D. Baker, and W.A. Catterall. 2012. Structural basis for gating charge movement in the voltage sensor of a sodium channel. *Proc. Natl. Acad. Sci. USA.* 109:E93–E102. http://dx.doi.org/10.1073/pnas.1118434109

Zhao, Y., S. Araki, J. Wu, T. Teramoto, Y.F. Chang, M. Nakano, A.S. Abdelfattah, M. Fujiwara, T. Ishihara, T. Nagai, and R.E. Campbell. 2011. An expanded palette of genetically encoded Ca^{2+} indicators. *Science.* 333:1888–1891. http://dx.doi.org/10.1126/science.1208592